
Journal of Computational Neuroscience 9, 5–30, 2000

A Temporal Mechanism for Generating the Phase Precession of Hippocampal Place Cells

AMITABHA BOSE, VICTORIA BOOTH AND MICHAEL RECCE
Department of Mathematical Sciences, Center for Applied Mathematics and Statistics, New Jersey Institute of Technology, Newark, NJ, 07102-1982
bose@nimbu.njit.edu

Received December 1, 1998; Revised June 21, 1999; Accepted June 25, 1999

Action Editor: John Rinzel

Abstract. The phase relationship between the activity of hippocampal place cells and the hippocampal theta rhythm systematically precesses as the animal runs through the region in an environment called the *place field* of the cell. We present a minimal biophysical model of the phase precession of place cells in region CA3 of the hippocampus. The model describes the dynamics of two coupled point neurons—namely, a pyramidal cell and an interneuron, the latter of which is driven by a pacemaker input. Outside of the place field, the network displays a stable, background firing pattern that is locked to the theta rhythm. The pacemaker input drives the interneuron, which in turn activates the pyramidal cell. A single stimulus to the pyramidal cell from the dentate gyrus, simulating entrance into the place field, reorganizes the functional roles of the cells in the network for a number of cycles of the theta rhythm. In the reorganized network, the pyramidal cell drives the interneuron at a higher frequency than the theta frequency, thus causing a systematic precession relative to the theta input. The frequency of the pyramidal cell can vary to account for changes in the animal's running speed. The transient dynamics end after up to 360 degrees of phase precession when the pacemaker input to the interneuron occurs at a phase to return the network to the stable background firing pattern, thus signaling the end of the place field. Our model, in contrast to others, reports that phase precession is a temporally, and not spatially, controlled process. We also predict that like pyramidal cells, interneurons phase precess. Our model provides a mechanism for shutting off place cell firing after the animal has crossed the place field, and it explains the observed nearly 360 degrees of phase precession. We also describe how this model is consistent with a proposed autoassociative memory role of the CA3 region.

Keywords: phase precession, minimal biophysical model, place cells, theta rhythm

1. Introduction

There is considerable current interest in the ways in which the temporal firing pattern of neurons may provide additional information that is not conveyed by the averaged firing rate alone. This interest has led to a search for ways in which temporal firing properties of neurons are generated and detected in the central nervous system (for a review, see Rieke et al., 1997; Recce, 1999). The main goal of this article is to use minimal biophysical modeling to demonstrate how a group of neurons in region CA3 of the hippocampus of freely moving rats can generate a spatially encoded output, called *phase precession*, using only limited and spatially nonspecific inputs.

It has been proposed that hippocampal place cells provide information for downstream neurons through the phase relationship between neuronal activity and the hippocampal EEG (O'Keefe and Recce, 1993). Place cells were first described in the CA1 region of freely moving rats (O'Keefe and Dostrovsky, 1971), and the activity of these putative pyramidal cells (Fox

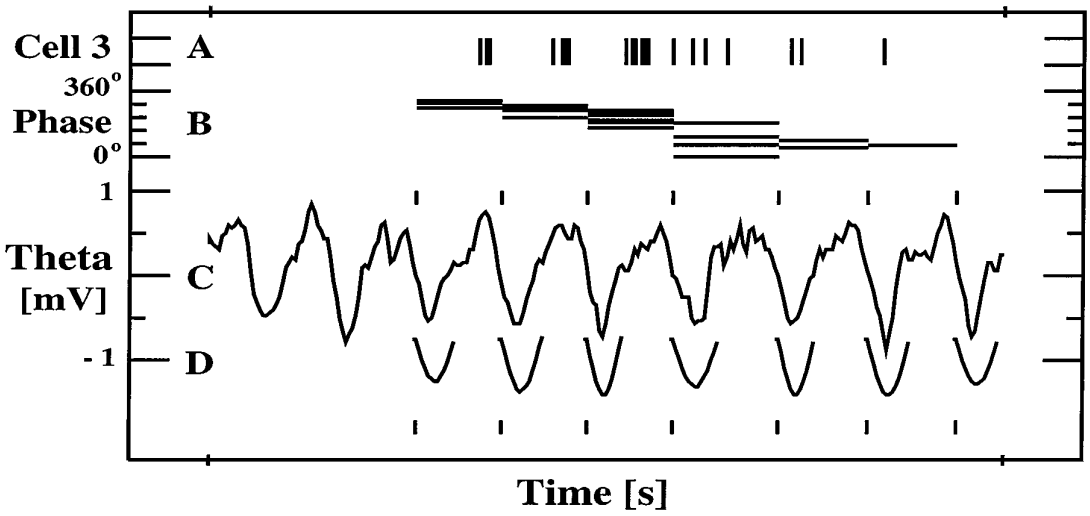

Figure 1. Extraction of the firing phase shift for each spike during a single run through the place field of a place cell on the linear runway. A: Each action potential from cell 3 during the one second of data shown in the figure is marked with a vertical line. B: The phase of each spike relative to the hippocampal theta rhythm. C: Hippocampal theta activity recorded at the same time as the hippocampal unit. D: Half sine wave fit to the theta rhythm that was used to find the beginning of each theta cycle (shown with vertical ticks above and below the theta rhythm). Reprinted from O'Keefe and Recce (1993).

and Ranck, 1975) is highly correlated with the rat's location in an environment (O'Keefe, 1976; Muller et al., 1987). The preferred firing location of a place cell is called its *place field*.

During locomotor activity, the hippocampal EEG has a characteristic 6 to 12 Hertz sinusoidal form called the *theta rhythm* (Green and Arduini, 1954), and the phase and frequency of this rhythm is highly correlated across the CA1 region of the hippocampus (Bullock et al., 1990). As the rat runs through a place field, on a linear runway, the phase of the theta rhythm at which a place cell fires systematically precesses. Each time the animal enters the place field, the firing begins at the same phase, and over the next five to ten cycles of the theta rhythm it undergoes up to 360 degrees of phase precession (O'Keefe and Recce, 1993; Skaggs et al., 1996). The maximum observed phase precession was 355 degrees (O'Keefe and Recce, 1993). So, by the phrase "up to 360 degrees of phase precession" we mean strictly less than but in a neighborhood of 360 degrees. An example of the phase precession of a place cell is shown in Fig. 1. During the run along the track, the phase of hippocampal place cell firing is more correlated with the animal's location within the place field than with the time that has passed since it entered the place field (O'Keefe and Recce, 1993). This suggests that the phase of place cell activity provides more information on the location than is available from the firing rate of the cell alone. A downstream system that measures the phase of place cell activity would then have more information about the location of the animal in the environment and may be able to ignore out of place field firing that occurs preferentially at a phase that is different from the range found in the place field. Place cells in both the CA1 region and the upstream CA3 region are found to undergo phase precession (O'Keefe and Recce, 1993).

Skaggs and coworkers (1996) confirmed this finding and additionally found that the initial phase was consistent among a large number of place cells in the CA1 region. They also found that dentate granule cells that project to CA3 undergo a small number of cycles of phase precession and therefore provide a synchronized, timed excitation to the CA3 pyramidal cells. Marr (1971) proposed that this input from the dentate granule cells provides a seed input for a memory retrieval and pattern completion process that is driven by the excitatory feedback among pyramidal cells in the CA3 region (Treves and Rolls, 1994; Gibson and Robinson, 1992; Hirase and Recce, 1996). The phase precession of place cells may be an essential part of this pattern completion process.

The hippocampal regions also contain a variety of interneurons that contribute to the generation of hippocampal oscillations. These interneurons project to place cells as well as to other interneurons (Freund

and Buzsáki, 1996). Skaggs and coworkers (1996) measured the phase of interneuron firing in the CA1 region and found that on average the interneurons do not phase shift. On the other hand, Csicsvari and coworkers (1998) found a large, significant cross-correlation between pyramidal cell and interneuron pairs, where the pyramidal cell firing precedes interneuron firing by tens of milliseconds. This implied high synaptic conductance from pyramidal cells to interneurons suggests that interneurons could phase precess. This suggestion may not be inconsistent with the experimentally observed average properties of interneurons (Skaggs et al., 1996) if only a subset is shown to transiently phase precess.

The medial septum is also involved in modulating the temporal firing patterns of hippocampal place cells and interneurons. The projection from the medial septum to the hippocampus is both GABAergic and Cholinergic (Freund and Antal, 1988), and it provides a pacemaker to drive the theta rhythm (Green and Arduini, 1954). We have shown that the interburst frequency of some of the neurons in the medial septum is a linear function of a rat's running speed on a linear track (King et al., 1998).

In summary, the observed properties of the phase precession phenomenon include the following: (1) place cells fire in only one direction of motion during running on a linear track; (2) all place cells start firing at the same initial phase; (3) the initial phase is the same on each entry of the rat into the place field of a place cell; (4) the total amount of phase precession is always less than 360 degrees; (5) the cells in the dentate gyrus that project to CA3 undergo a smaller number of cycles of phase precession; (6) in one-dimensional environments, the phase plus firing rate provide more information of the rat's location than the firing rate of a place cell; (7) phase is more correlated with the animal's location in a place field than with the time since the animal entered the place field; and (8) background firing of place cells outside of the place field occurs at a fixed phase that is closest to the initial phase that occurs when the animal enters the place field.

Several models have been proposed to explain the neural basis of the phase precession phenomenon. The model proposed by Tsodyks and coworkers (1996) provides an environment-driven phase precession, which is certain to be more correlated with position than time. Other models of environment-driven phase precession have been proposed by Wallenstein and Hasselmo (1997) and Jensen and Lisman (1996). In these models, the phase correlation in CA1 pyramidal cells results from CA3 input that is phase precessing. Kamondi and coworkers (1998) have proposed a model for phase precession in the CA1 region that does not depend on precisely timed inputs, but instead the phase is a result of the total amount of depolarization of the place cells. In this model, the total amount of phase shift is much less than 360 degrees.

In this article, we describe a minimal biophysical temporal model for phase precession in the CA3 region of the hippocampus. It differs from prior models in that (1) it generates the spatial correlation of the phase precession from a single spatial input and from information about the animal's running speed; (2) it does not require phase precession in the upstream projection cells; (3) it does not require a spatially dependent depolarization of place cells; (4) it provides a mechanism for determining the end of the place field; (5) it provides a mechanism for up to 360 degrees of phase shift; and (6) it is consistent with associative memory models for the CA3 region.

Alternatively, our model does not include a mechanism to account for the firing rate of place cells. The activity of place cells includes both rate and timing information. In the present model, we are only concerned with the timing properties.

This minimal model, which is composed of two neurons (one pyramidal cell and one interneuron) and a pacemaker input, can explain the onset, occurrence, and end-of-phase precession. The network has two important dynamic patterns. The first is a stable attracting state, which mimics the behavior of CA3 outside of the place field. The second dynamic pattern is a transient state that encodes the behavior of CA3 within the place field. The main difference between the two states is the input that controls the firing pattern of the interneuron. In the stable state, the pacemaker input controls interneuron firing, while in the transient state, excitation from the pyramidal cell does. The seed from the dentate gyrus switches control from the pacemaker to the place cell to initiate phase precession, and the duration of phase precession is determined by the duration of the transient dynamics as the network returns to the stable state.

The transient place cell firing in the place field is a temporal process in which the phase of firing of the cell in each cycle of the theta rhythm strictly depends on the phase in the prior cycle of the theta rhythm. This is in contrast to all other models of phase precession in which the phase of firing of place cells depends on the external inputs arriving at that cycle and not on the phase in other cycles of the theta rhythm. For this reason, to account for the spatial correlation of phase

precession, the present model requires that the amount of phase change during a theta cycle depends linearly on changes in the animal's running speed. Neurons in the medial septum have been found to have an interburst frequency that is a linear function of the running speed of a rat (King et al., 1998). Also, the theta frequency in the hippocampus of rats running on a linear track has been found to be highly correlated with the rat's speed (Recce, 1994). Since the phase-precession data includes a range of running speeds (O'Keefe and Recce, 1993), this implies the interburst frequency of place cells is also a function of the animal's running speed. These data provide a mechanism to maintain a spatially correlated phase precession in the proposed temporal model.

The model generates two different types of spatial information. First, it determines the length of the place field. The place field ends when phase precession ends, which occurs when the pacemaker regains control of the interneuron from the place cell. Second, the model determines the location of the animal within the place field. Note that these two types of spatial information are generated from the seed, a single location specific input, and the velocity of the animal, a nonspatially specific input.

Our model supports two themes that have arisen in other neural modeling studies. The first is that the control of the dynamics in a network may switch among different neurons over time. These switches can occur in the absence of any synaptic changes. Instead, dynamics are governed by the timing of events relative to one another (Ermentrout and Kopell, 1998; Nadim et al., 1998). The second theme concerns the role of inhibition in networks of neurons. In recent studies (Terman et al., 1998; Rubin and Terman, 1999; van Vreeswijk et al., 1994), it is shown that inhibition may have counterintuitive effects on the network, such as synchronizing mutually coupled inhibitory cells. In the present study, we use inhibition to *speed up* the oscillations of the pyramidal cell.

The primary prediction of this model is that phase precession is a spatially specific output that results from an integration of a spatial signal from the dentate gyrus at a single point and a nonspatial velocity coded signal originating from the medial septum. We predict that no upstream physiological signal exists that contains as much information about the animal's spatial location as the phase of hippocampal place cell firing in CA3. This prediction differentiates our model from all other models of phase precession that require an input that is as spatially precise as the phase precessing output. Another prediction, which is easier to address experimentally, is that a subset of the interneurons transiently phase precesses. The model also strongly depends on, and thus predicts, continued evidence for a linear frequency dependence of pyramidal cells in CA3 and projection cells in the medial septum on running speed of the animal.

2. Model and Methods

2.1. Model

Our minimal biophysical model for phase precession in CA3 consists of a pyramidal or place cell, an interneuron, and a pacemaker input, denoted P, I, and T, respectively. The pacemaker input T may be thought of as an individual cell or perhaps a conglomeration of inputs that produce the theta rhythm. The synaptic connections among P, I, and T reflect the network architecture of CA3 (see Fig. 2). Specifically, the pyramidal cell P receives fast, GABA-mediated inhibition from the interneuron I and projects to I via fast, glutamatergic excitation. The pacemaker input

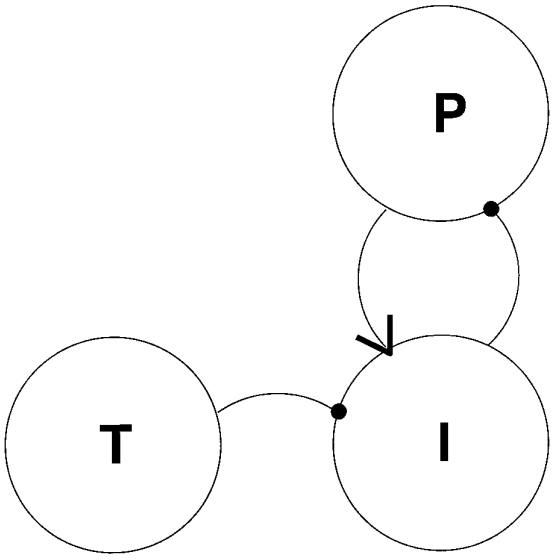

Figure 2. Two cell and pacemaker network model consisting of a pyramidal or place cell (P), an interneuron (I), and a pacemaker input (T). Synaptic connections reflect CA3 network architecture (arrow indicates excitatory and filled circle indicates inhibitory synaptic connections).

T projects only to I through fast, GABA-mediated inhibition.

Our analysis does not depend on a specific model for the individual neurons; hence, we use a general form for the model equations for each cell. The few restrictions we require on the model properties (outlined below) are satisfied by a large class of neural oscillators, including the Morris-Lecar (Morris and Lecar, 1981) equations, which have been successfully used in numerous modeling studies (Rinzel and Ermentrout, 1997; Somers and Kopell, 1993; Terman et al., 1998; Terman and Lee, 1997), and which we use for our simulations (see Appendix B).

The P cell is a general neural oscillator, modeled by equations of the following form:

$$\begin{aligned} v_p' &= f_p(v_p, w_p) \\ w_p' &= \epsilon g_p(v_p, w_p), \end{aligned} \tag{1}$$

where $'$ denotes the derivative with respect to time t. The variable v_p represents the membrane voltage of the place cell and the function f_p is composed of the sum of the ionic and leakage currents found in the cell as well as an applied current. We consider P to have bursting behavior and the variable v_p to model the burst envelope and not to account for individual, fast spikes occurring during the active phase of the burst. In this general class of neural models, the variable w_p models the activation gating variable of an outward, ionic current, usually potassium-mediated, and the function g_p governs the activation gate dynamics of this conductance. The parameter ϵ controls the time scale of the w_p dynamics. Our analysis assumes that ϵ is small ($\epsilon \ll 1$), so that this general neural oscillator behaves as a relaxation oscillator.

The model for the interneuron I also has a general form, but we consider I to be an excitable cell, rather than oscillatory. The model equations are

$$\begin{aligned} v_i' &= f_i(v_i, w_i) \\ w_i' &= \epsilon g_i(v_i, w_i), \end{aligned} \tag{2}$$

where v_i represents the membrane voltage of I and w_i represents the activation gating variable of an outward, ionic current. As described below in terms of its phase plane, we require that it is able to fire in response to either excitation received from P or inhibition received from T.

The equations for the pacemaker T are completely general. In fact, we simply assume that T oscillates between 0 and 1, with a period T_T in the theta range. When the value of T exceeds a prescribed threshold, then we assume that T fires, and we measure the duration of its "spike" as the time spent above the threshold.

For the network model, appropriate synaptic currents are added to the individual cell models. In the synaptic current variables and parameters, the first subscript denotes the presynaptic cell and the second subscript denotes the postsynaptic cell. The network equations for P are

$$\begin{aligned} v_p' &= f_p(v_p, w_p) - g_{ip} s_{ip}(t - \sigma_{ip})[v_p - v_{ip}], \\ w_p' &= \epsilon g_p(v_p, w_p). \end{aligned} \tag{3}$$

For I, the network equations are

$$\begin{aligned} v_i' &= f_i(v_i, w_i) - g_{pi} s_{pi}(t - \sigma_{pi})[v_i - v_{pi}] \\ &\quad - g_{ti} s_{ti}(v_i - v_{ti}), \\ w_i' &= \epsilon g_i(v_i, w_i). \end{aligned} \tag{4}$$

This form of the synaptic currents has been used in other modeling studies (Ermentrout and Kopell, 1998; Wang and Rinzel, 1992). The variables s_{ip}, s_{pi}, and s_{ti} govern the dynamics of the synaptic currents, and each satisfies an equation of the form

$$s' = \alpha H_\infty(v - v_\theta)(1 - s) - \beta s, \tag{5}$$

where α and β are the rise and decay rates of the synapse, and v_θ is the synaptic activation threshold. The Heaviside step function H_∞ acts as an activation switch for the synapse; $H_\infty(v - v_\theta)$ is 0 if $v < v_\theta$ and is 1 if $v \geq v_\theta$. The parameters g_{pi}, g_{ti}, and g_{ip} are the maximal conductances of these synaptic currents, and v_{pi}, v_{ti}, and v_{ip} are the reversal potentials. In particular, v_{ip} and v_{ti} are set to make the associated currents outward, while v_{pi} is set to make the synaptic current inward. Finally, the parameters σ_{ip} and σ_{pi} represent a synaptic delay from I to P and P to I, respectively. Without loss of generality, we assume there is no delay between T and I.

2.2. Phase Plane Methods

In this section, we describe the phase plane methods we use to analyze the model. We first explain how the behavior of each cell when isolated from the network can be studied in the phase plane and then describe the effect of network interactions. An important aspect

of our analysis that is worth mentioning at this initial stage is that we often compare behavior of uncoupled and coupled versions of P. By the former, we mean the intrinsic P cell oscillation in isolation from the network. By the latter, we mean the oscillation of the same P cell when it must now interact with T and I in the network. One of the important conclusions of our analysis is that the network dynamics can evolve in dramatically different ways, depending on the firing sequence of the cells.

The oscillatory behavior of the isolated P cell can be analyzed in the $v_p - w_p$ phase plane where the trajectory of the cell is determined by the nullclines of each equation (see Fig. 3). The v_p-nullcline, denoted C_P, is a cubic-shaped or N-shaped curve found by solving $f_p(v_p, w_p) = 0$ for w_p. The w_p-nullcline, denoted D_P, is a sigmoidal-shaped, nondecreasing curve found by solving $g_p(v_p, w_p) = 0$. To ensure that the isolated P cell is oscillatory, parameters in the functions f_p and g_p are chosen so that C_P and D_P intersect uniquely along the middle branch of C_P. As in prior models (Somers and Kopell, 1993; Terman and Lee, 1997; Terman et al., 1998), we require that the following condition on g_p holds near the left branch of C_P:

$$\frac{\partial g_p}{\partial v_p} > 0. \tag{6}$$

Following standard analysis of relaxation oscillators, in the limit $\epsilon = 0$, the burst trajectory of the P cell can be traced in the phase plane. As displayed in Fig. 3, the silent phase of the burst occurs as the trajectory travels down the left-hand branch of the cubic-shaped nullcline C_P, while during the active phase of the burst, the trajectory travels up the right-hand branch of C_P. The transitions between the active and silent phases of the oscillation occur when the trajectory reaches the knees of the nullcline. One cycle of the burst oscillation is obtained by tracing along the four different "pieces" of the trajectory. Specifically, setting $\epsilon = 0$ in (1), we obtain the following, fast equations governing the transitions of the P cell between its active and silent states:

$$\begin{aligned} v_p' &= f_p(v_p, w_p) \\ w_p' &= 0. \end{aligned} \tag{7}$$

In this case, w_p acts as a parameter in the v_p equation, which is simply a scalar equation and thus easy to analyze. The equations governing the slow variation of v_p during its active and silent states are obtained by rescaling time using $\tau = \epsilon t$ in (1) and then setting $\epsilon = 0$:

$$\begin{aligned} 0 &= f_p(v_p, w_p) \\ \dot{w}_p &= g_p(v_p, w_p), \end{aligned} \tag{8}$$

where $\dot{}$ denotes the derivative with respect to the slow time variable τ. To mathematically construct the oscillation cycle, we denote the left and right knees of the nullcline C_P by (v_{LK}, w_{LK}) and (v_{RK}, w_{RK}) respectively. Results by Mishchenko and Rozov (1980) imply that for ϵ sufficiently small, an actual periodic orbit lies $O(\epsilon)$ close to a so-called singular periodic orbit. The singular periodic orbit consists of four pieces, all of which are constructed with $\epsilon = 0$. The first is a solution of (7) that connects (v_{LK}, w_{LK}) to some point (v_R, w_{LK}) on the right branch of C_P (rising edge of burst). The next piece is a solution of (8) that connects (v_R, w_{LK}) to (v_{RK}, w_{RK}) (active phase of burst). The third piece is a solution of (7) that connects (v_{RK}, w_{RK}) to (v_L, w_{RK}) (falling edge of burst). The final piece is a solution of (8) that connects (v_L, w_{RK}) back to (v_{LK}, w_{LK}) (silent phase). Note that with respect to the slow time scale τ, the jumps between the active and silent states of the burst are instantaneous. We denote the period of the singular periodic orbit by T_P.

The nullclines for the model interneuron with excitable behavior have the same qualitative shape as those for the P cell, except model parameters are adjusted so that the cubic-shaped v_i-nullcline, denoted C_I, and the sigmoidal w_i-nullcline, D_I, intersect along the left branch of C_I. The intersection point of the nullclines is a stable fixed point along the left-hand resting branch of C_I, that ensures that the isolated I cell is unable to oscillate on its own. This change in the nullclines can be obtained, for example, by shifting the half-activation voltage of the outward current to lower voltage levels. A property we assume for the intersection point of the nullclines is that this point be close to the left knee of the nullcline C_I, thus allowing the interneuron to fire either in response to excitation from the P cell or via rebound following inhibition from the pacemaker T. As with P, we assume that near the left branch of C_I,

$$\frac{\partial g_i}{\partial v_i} > 0. \tag{9}$$

In our geometric analysis in the phase plane, the general effect of introducing a synaptic current is to either raise or lower the cubic-shaped nullcline of

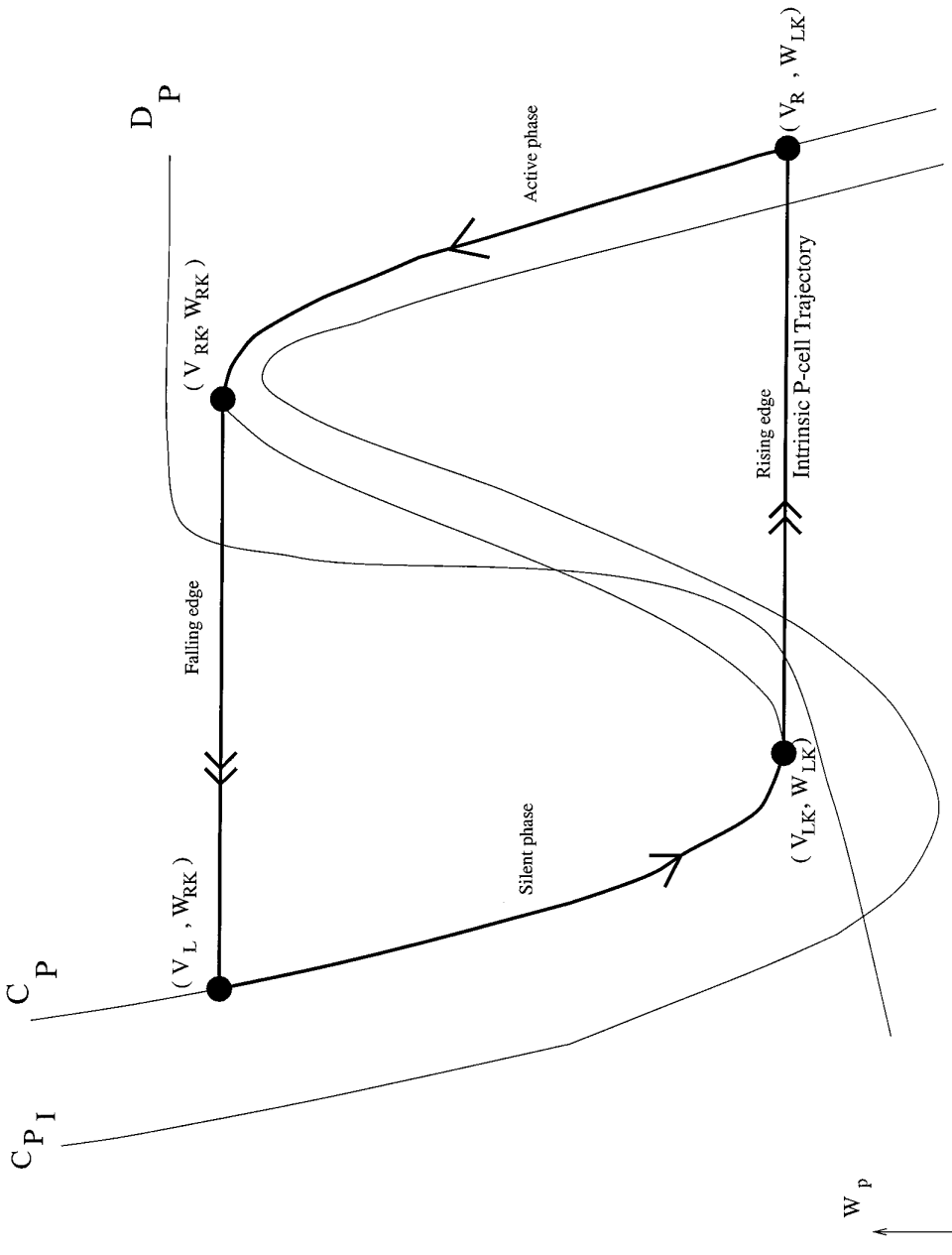

Figure 3. The nullclines C_P, C_{P_I}, and D_P are depicted. The intrinsic trajectory of the P cell is superimposed on C_P. A single arrow denotes a slow flow, while a double arrow denotes a fast jump. These fast jumps are instantaneous with respect to the slow flow.

the postsynaptic cell without qualitatively changing its shape, as long as the maximum synaptic conductance is not too large relative to the maximum ionic conductances. Since (5) contains no factor of ϵ, the synapses turn on and off on the fast time scale governed by t; thus they are instantaneous with respect to the slow flow of the trajectories governed by τ. To examine the effects of the synaptic currents on the P cell in our network model, we denote the solution curve of $f_p(v_p, w_p) - s_{ip}(t - \sigma_{ip})g_{ip}[v_p - v_{ip}] = 0$ by C_{P_I}. Since P receives inhibition, C_{P_I} lies below C_P (see Fig. 3). We assume that the nullcline D_P and C_{P_I} intersect somewhere along the left branch of C_{P_I}. This intersection point will be a stable fixed point for the inhibited P cell, with the result that the inhibited P cell will not spontaneously oscillate. Further note that this intersection point will lie below the left knee of C_P because of our restriction (6) $\frac{\partial g_p}{\partial v_p} > 0$ (see Somers and Kopell, 1993).

The effect on I of the excitatory synaptic current from P and the inhibitory synaptic current from T is that its cubic-shaped nullcline can be raised or lowered depending on the activation of s_{pi} and s_{ti}. For any possible case, we assume that the w_i-nullcline D_I continues to intersect the synaptically perturbed v_i-nullclines along their left branches, thus ensuring that I remains excitable. As noted previously, we require that I be able to fire due to either excitation received from P or via rebound from inhibition received from T. For example, assume that I is sufficiently close to the intersection point of the nullclines when it receives synaptic input. If the input is excitatory from P, the cubic-shaped nullcline of the I cell is instantaneously raised releasing the trajectory from its left branch. The trajectory is then attracted to the right branch of the raised nullcline, thus initiating an action potential. If the input is inhibitory from T, the cubic-shaped nullcline is lowered and the trajectory moves left toward the new stable fixed point at the intersection of the perturbed nullcline and D_I. For sufficiently strong inhibition, because of our restriction (9), the new fixed point will lie below the left knee of C_I. When the synaptic inhibition shuts off, the nullcline rises back again toward C_I, and the trajectory is attracted to the right branch, initiating an action potential via postinhibitory rebound. The ability of the I cell to fire due to these two different stimuli is critical to our analysis.

The mathematical analysis for this article, as well as the specific equations used in the simulations, can be found in Appendices A and B, respectively. We work throughout in the appropriate $\epsilon = 0$ limit and then use results of Mischenko and Rozov (1980) to obtain the ϵ small result. Our proofs depend on the use of a time metric that allows us to define times between cells and also times over which relevant behavior occurs. It turns out that we can relate many of the times associated with the network model back to times associated with the isolated cells.

3. Results

3.1. System Properties

We first present an overview of our results that provides a qualitative description of how and why the model generates phase precession. In the second part of this section, we provide the analysis of our model and specific analytical results.

There exist two different, important firing patterns for the simple network. The first firing pattern represents network behavior when the rat is outside of the place field. The second represents network behavior when the rat is inside the place field. The difference between these two behaviors is directly correlated to whether T or P controls the firing of I. An important aspect of our analysis is to identify mechanisms that allow the control of firing to be shifted between T and P. As described below, the first change in control from T to P requires a brief external input to the network occurring when the rat first enters the place field. The second change in control from P back to T is determined internally by the network and signals that the place field has ended.

The firing pattern representing out-of-place field behavior is a stable periodic state that we call the *TIP* orbit. In this stable pattern, the pacemaker T controls the firing of I, which fires via postinhibitory rebound. In turn, I modulates the firing of P, so that it fires phase-locked to the underlying theta rhythm. The effect of the inhibition from I is to either delay or advance the firing of P, depending on where in P's cycle the inhibition occurs. Thus, P is phase-locked to the theta rhythm and does not phase precess whether its intrinsic frequency is higher or lower than theta (see Section 3.2.1). Moreover, P can only fire when released from inhibition from I.

Simulation results from the simple network where each cell is modeled with Morris-Lecar equations are shown in Fig. 4. During the first five bursts of the P cell (top trace), the network is in the stable *TIP* orbit. The

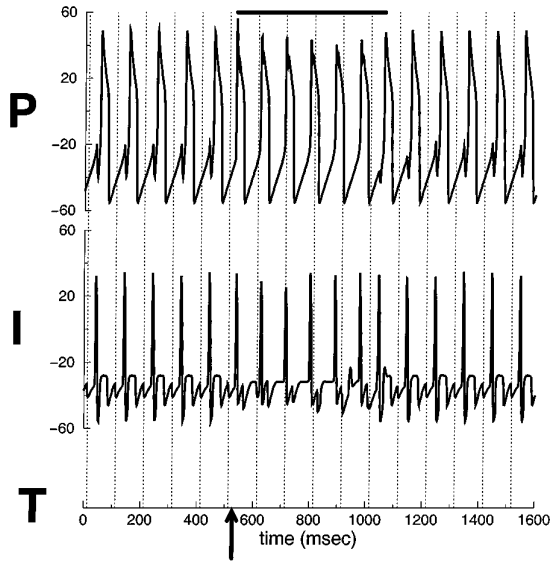

Figure 4. *TIP* and *PIT* orbits for the two cell and pacemaker network with each cell modeled by Morris-Lecar equations. The T spike is not explicitly shown and is denoted by dashed vertical lines. The network oscillates in the *TIP* orbit for the first 5 cycles. The *PIT* orbit is initiated by the arrival of the memory seed (heavy arrow at 535 msec, which lasts for 3 msec) and phase precession occurs over the next 7 cycles (under heavy bar). The network returns to the stable *TIP* orbit for the remainder of the simulation. The model equations and parameter values are given in Appendix B.

sequence of cell firing with T firing first (not explicitly shown; time of peak indicated by dotted vertical lines), followed by I (lower trace) and then P is evident. During the T spike, I is inhibited as seen by the hyperpolarization in the I voltage trace immediately following the peak of T. During the I spike (after its release from inhibition from T), P is inhibited as seen by the hyperpolarization in the P voltage trace immediately preceding the spike.

Clearly, the out-of-place field firing rate in the *TIP* orbit is higher than experimentally observed. This high out-of-place field firing leads to a loss of spatial specificity to a downstream detector of firing rate but has minimal effect on a downstream detector that uses the phase of firing to determine the spatial location of the animal. The simplest way to reduce or remove the out-of-place field firing is to have a spatial inhibitory signal that provides inhibition at all points outside of the place field. This approach is not taken here because it relies on spatial information upstream from the hippocampus about the size and extent of the place field. The goal of this model is to generate the spatial phase correlation from less spatially specific upstream information. Following the description of the properties of the simple model, we show in Section 3.2.7 how to completely suppress the out-of-place field firing, without resorting to additional upstream spatial information (see Fig. 9).

The second firing pattern, representing behavior within the place field, is a transient state that we call the *PIT* orbit. The *PIT* orbit is initiated by a brief, solitary dose of excitation to P, representing a memory seed externally provided from the dentate gyrus. The seed causes P to fire earlier than it would have in the *TIP* orbit and thereby allows P to seize control of I's firing. The P cell is able to fire via its intrinsic oscillatory mechanisms for as long as it controls I. Thus, the seed has the effect of switching control of I from T to P. During the *PIT* orbit, the period of P firing, T_P, is less than the period of T, T_T, regardless of the intrinsic period of P, provided that T_P and T_T are not too disparate. The reason phase precession occurs in the *PIT* orbit is somewhat subtle and depends both on the intrinsic periods of P and T and also on the time duration of inhibition from I to P. If this inhibition is short-lasting, then during *PIT*, P fires at its intrinsic frequency. Thus if $T_P < T_T$, it is clear that precession will occur. Alternatively, if the inhibition is long-lasting, then during *PIT*, P fires at a substantially faster rate than its intrinsic frequency. Counterintuitively, this increase in firing rate is most strongly dependent on the strength of the inhibitory synaptic conductance from I to P. In Section 3.2.2, we clarify how inhibition may speed up the firing rate of P. For this case, precession occurs whether the intrinsic period T_P is less than, greater than or equal to T_T. In either case, since P controls the firing of I in the *PIT* orbit, forcing I to fire with every P burst, I also phase precesses.

Figure 4 illustrates the *PIT* orbit and phase precession for the Morris-Lecar model network. Arrival of the memory seed to P is modeled by a brief, excitatory, applied current pulse (heavy arrow) that causes the early firing of P and the interruption of the *TIP* orbit. Due to the excitation from P, I overcomes the inhibition from T and fires with P, as seen by the slight hyperpolarization in the peak of the P burst. Over the next six cycles (under the heavy bar), P and I phase precess relative to T. The firing of P due to intrinsic oscillatory mechanisms is evidenced by the smooth rise to threshold displayed by its voltage trace.

The phase precession of I provides an internal mechanism that returns the network to the *TIP* orbit. Namely,

in *PIT*, I continues to receive inhibition with each T spike, but the timing or phasing of the inhibition is such that postinhibitory rebound does not occur at each cycle. For example, during the first two spikes of phase precession, the inhibition from T arrives during the I spike, as seen by the lower spike heights, and rebound does not occur. Over the next three cycles, T inhibits I during early portions of its afterhyperpolarization when rebound is not possible. But by the last spike of phase precession, I is inhibited sufficiently late in its afterhyperpolarization, resulting in a rebound spike that interrupts the *PIT* orbit, returning the network to the stable *TIP* orbit. The recapture of I by T signals the end of the place field and occurs when P and I have precessed through up to 360 degrees of phase, which is consistent with experimental data (O'Keefe and Recce, 1993). Thus, the precession of I is necessary for determining the end of the place field.

The brief dose of excitation in the form of the memory seed reorganizes the functional roles of the cells in the *TIP* and *PIT* orbits. Namely, the excitation switches the control of I from T to P. T is able to regain control of I only when P and I have precessed through up to 360 degrees. Note that this functional reorganization occurs without any changes in the coupling or intrinsic properties of the cells. We emphasize that, in the model, phase precession is a transient phenomena that ceases with no further input to the network. Thus, the length of time over which the pyramidal cell precesses, or alternatively, the length in space over which precession occurs, completely determines the spatial extent of the place field. In this way, the network generates the temporal code embodied in phase precession.

In the following analytic results section, we provide mathematical justification for the qualitative observations described here (see Table 1 for a list of relevant symbols). In particular, in Section 3.2.1, we discuss the existence of the *TIP* orbit. In Sections 3.2.2 to 3.2.5, we focus on the *PIT* orbit and determine parameters that most strongly affect this network behavior. In Section 3.2.6, we show how experimentally supported data relating running speed to interburst frequency of the pyramidal cells can be used to achieve a spatial correlation in this temporal model. Finally in Section 3.2.7, we introduce a modification to the simple network that suppresses out-of-place field firing.

3.2. Analysis

3.2.1. The Network Oscillates at Theta Frequency Outside of the Place Field. The trajectories of P and I in the *TIP* orbit can be traced along nullclines in their phase planes. We may assume that at $\tau = 0$, T fires, the trajectory of P lies on the left branch of C_P with $w_p(0) = w^\star$ and the trajectory of I lies somewhere along the left branch of C_I. In response to the inhibition received from T, I falls back to C_{I_T} and is released from inhibition at $\tau = \tau_{T_{on}}$. We assume that $w_i(0)$ is such that $w_i(\tau_{T_{on}})$ lies below the left knee of C_I. Thus at $\tau = \tau_{T_{on}}$, I fires by postinhibitory rebound. Allowing for synaptic delay from I to P, at $\tau = \tau_{T_{on}} + \sigma_{ip}$, P feels inhibition from I and as a result falls back to C_{P_I}. At $\tau = \tau_{T_{on}} + \sigma_{ip} + \tau_{I_{on}}$, P is released from inhibition. We show in Appendix A that $w^\star$ can be chosen such that $w_p(\tau_{T_{on}} + \sigma_{ip} + \tau_{I_{on}}) < w_{LK}$. With this condition, when P is released from inhibition, it will fire. Depending on the position of the trajectory of P on the left branch of C_P when the inhibition from I arrives, at $\tau = \tau_{T_{on}} + \sigma_{ip}$, the firing of P has either been delayed or advanced relative to its intrinsic frequency. We also show in Appendix A that when T fires again at $\tau = T_T$, $w_p(T_T) = w^\star$, thus ensuring that this cycle of firing repeats, and we show that the *TIP* orbit is stable. Note that for P to fire, it must be released from inhibition; it is unable to take advantage of the fact that it is an oscillatory cell.

In Fig. 5, we superimpose the phase portrait of the coupled P cell onto that of the uncoupled P cell to

Table 1. List of relevant symbols.

T_T = intrinsic period of the pacemaker input	C_P = intrinsic P cell cubic
T_P = intrinsic period of the P cell	C_I = intrinsic I cell cubic
$\Omega = T_T - T_P$	C_{P_I} = P cell cubic with $s_{ip} = 1$
T_{PC} = period of P cell in *TIP* network	C_{I_P} = I cell cubic with $s_{pi} = 1$
$T_{\bar{P}}$ = period of P cell in *PIT* network	C_{I_T} = I cell cubic with $s_{ti} = 1$.
$\tau_{T_{on}}$ = duration of the inhibition from T to I	$\tau_{I_{on}}$ = duration of inhibition from I to P
τ_{PA} = duration of the active state of the intrinsic P cell	τ_{PR} = duration of the silent phase of the intrinsic P cell
σ_{ip} = synaptic delay from I to P	σ_{pi} = synaptic delay from P to I

Note: All times are measured at $\epsilon = 0$ in slow time scale τ.

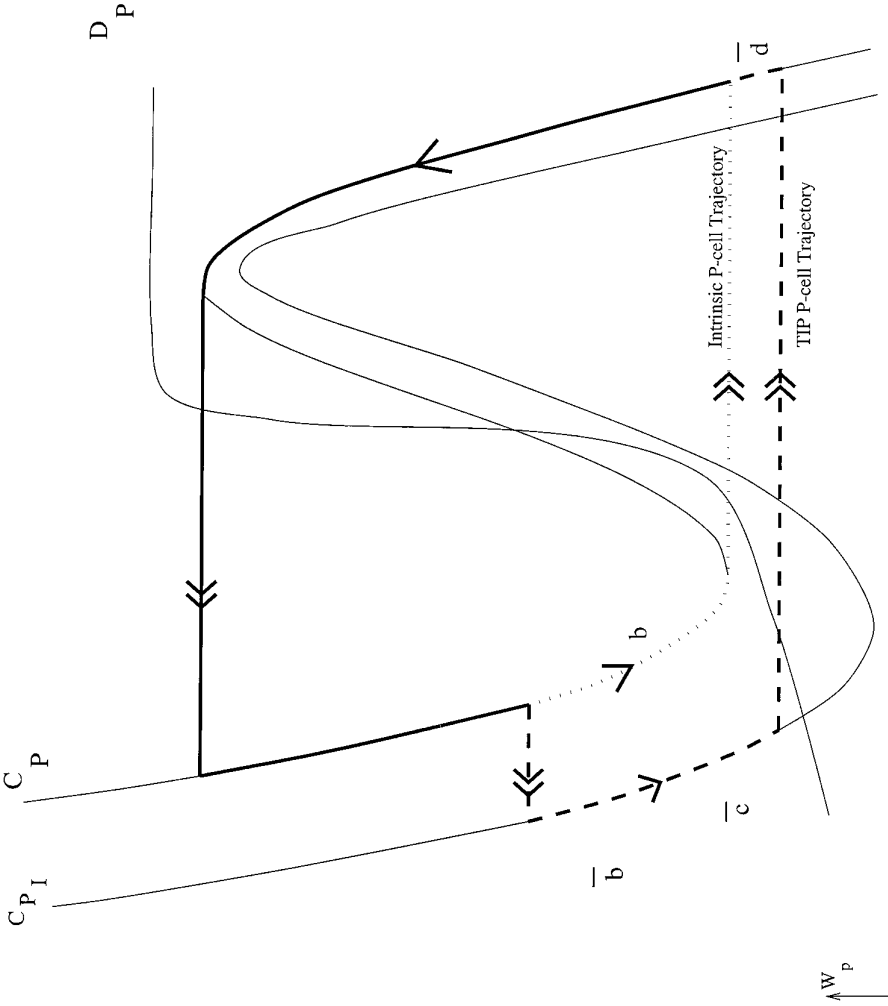

Figure 5. The coupled and uncoupled trajectories of the P cell are shown. The solid bold curves represent places in phase space where these two trajectories coincide. The dashed line corresponds to the coupled P cell, and the dotted line to the intrinsic P cell. The time b equals the time over the dotted part on C_P for the intrinsic P cell to reach the left knee of C_P. The time $\bar{b}$ is the time it takes the coupled P cell to cover the same vertical distance, but on the dashed part of the left branch of C_{P_I}. The time $\bar{c}$ equals the remaining time that the coupled P cell evolves along the dashed part of the left branch of C_{P_I}. The time $\bar{d}$ equals the time it takes to travel over the dashed part of the right branch of C_P.

clarify the differences in their trajectories. In the figure, we have used lowercase letters to denote times that these cells spend in parts of their orbit where their trajectories differ. The letters with bar superscripts correspond to the coupled P cell. Note that $T_{PC} - T_P = \bar{c} + \bar{d} - (b - \bar{b})$. Since $T_{PC} = T_T$, a necessary condition for the *TIP* orbit to exist is that the difference in intrinsic periods of P and T, $\Omega = T_T - T_P$, must satisfy

$$\Omega = \bar{c} + \bar{d} - (b - \bar{b}). \tag{10}$$

The difference $b - \bar{b} > 0$ is related to the magnitude of $\frac{\partial g_p}{\partial v_p}$. Since $\frac{\partial g_p}{\partial v_p} > 0$, cells evolve through the same Euclidean distance on C_P more slowly than on C_{P_l}. Thus $b - \bar{b}$ measures the additional time that the uncoupled P cell must spend to cover the same Euclidean distance along the left branch of C_P that the coupled P cell covers on C_{P_l}.

In the case when $\Omega > 0$, a stable *TIP* orbit is obtained if $\bar{c} + \bar{d} > b - \bar{b}$. This can be achieved by choosing $w_p(\tau_{T_{on}} + \sigma_{ip})$, and hence $w^\star$, such that the trajectory of P enters a neighborhood of the stable fixed point at the intersection of C_{P_l} and D_P within the duration of $\tau_{I_{on}}$. The trajectory of P will remain near the fixed point until P is released from inhibition. In this way, the firing of P is delayed and P can be phase-locked to the theta rhythm.

When $\Omega < 0$, a stable *TIP* orbit is achieved if $b - \bar{b} > \bar{c} + \bar{d}$. In this case, $w_p(\tau_{T_{on}} + \sigma_{ip})$, and hence $w^\star$, are chosen so that the trajectory of P remains sufficiently far from the fixed point at the intersection of C_{P_l} and D_P during $\tau_{I_{on}}$. The trajectory displayed in Fig. 5 is representative of this case. Since cells evolve faster on C_{P_l} than on C_P, the time $\bar{b} + \bar{c} + \bar{d}$ can be shorter than the time b. This shows that inhibition can be used to speed up P. Thus, P can be phase-locked to the theta rhythm if T_P is greater than T_T, as long as the periods are not too disparate.

Observe that (10) can also be rewritten as

$$\Omega = \tau_{I_{on}} + \bar{d} - b. \tag{11}$$

For fixed Ω, both b and $\bar{d}$ may increase as $\tau_{I_{on}}$ increases. An increase in b means that P must feel inhibition at higher values of w_P along the left branch of C_P. In turn, this means that in *TIP* the phase difference between T and P will be greater. Hence, the duration $\tau_{I_{on}}$ controls the phase difference between T and P in the *TIP* orbit.

In summary, the *TIP* orbit can be obtained whether the difference $\Omega = T_T - T_P$ is positive, negative, or zero. The effect of the inhibition from I to P depends not on its duration $\tau_{I_{on}}$ but on its timing during the cycle of P. We note that while the *TIP* orbit can be achieved with either positive or negative Ω, independent of the duration $\tau_{I_{on}}$, other results of our model—namely, obtaining the *PIT* orbit—require that for a short-lasting $\tau_{I_{on}}$, Ω must be positive.

3.2.2. Within the Place Field, Both P and I Phase Precess. Similar to above, we analyze the *PIT* orbit by describing the trajectories of P and I in their phase planes. In the following analysis, we assume that near the right branch of C_P, $\frac{\partial g_p}{\partial v_p} = 0$. Thus the speed at which P evolves along the right-hand branches of C_P and C_{P_l} will be the same. Our analysis continues to hold for $\frac{\partial g_p}{\partial v_p} > 0$ but sufficiently small. We also assume that near the right branch of C_I, $\frac{\partial g_i}{\partial v_p} = 0$.

For simplicity, we assume that the seed arrives at $\tau = 0$, so that both T and P fire simultaneously. The trajectory of P jumps to the right branch of C_P. The I cell receives inhibition from T during the time interval $(0, \tau_{T_{on}})$, but, at $\tau = \sigma_{pi}$, I fires due to excitation from P. At $\tau = \sigma_{pi} + \sigma_{ip}$, P receives inhibition from I and falls to the right branch of C_{P_l}. What happens next is most strongly determined by $\tau_{I_{on}}$, the time length over which P feels inhibition from I. The time $\tau_{I_{on}}$, however, is hard to define precisely as it changes during each cycle of the phase precession (see Appendix A for clarifications of this definition). We describe how the *PIT* orbit is obtained in the cases when $\tau_{I_{on}}$ is short and when it is long relative to the duration of the active state of P.

First consider the case when $\tau_{I_{on}}$ is short, in particular, $\tau_{I_{on}} < \tau_{PA}$, the duration of the active state of the uncoupled P cell. At $\tau = \sigma_{pi} + \sigma_{ip}$, let the distance along C_{P_l} from the position of the trajectory of P to the right knee be greater than $\tau_{I_{on}}$. Then the inhibition to P shuts off before P jumps down from the right knee of C_{P_l}. So at $\tau = \sigma_{pi} + \sigma_{ip} + \tau_{I_{on}}$, P returns to the right branch of C_P and leaves the active state through the right knee of its intrinsic cubic C_P. In Fig. 6A, we have drawn the trajectory that P follows one cycle after the seed is given. It follows this trajectory until the time at which the network returns to the *TIP* orbit. We denote by $T_{\bar{P}}$ the period of P during phase precession. In this case, $T_{\bar{P}} = T_P$. Thus, a necessary condition for phase precession in this scenario is $T_P < T_T$ or $\Omega > 0$. Here, the sole factor that drives the precession is the difference Ω in the intrinsic periods of P and T.

It is instructive to contrast the phase portrait of I with that of P during *PIT*. As opposed to the clean and

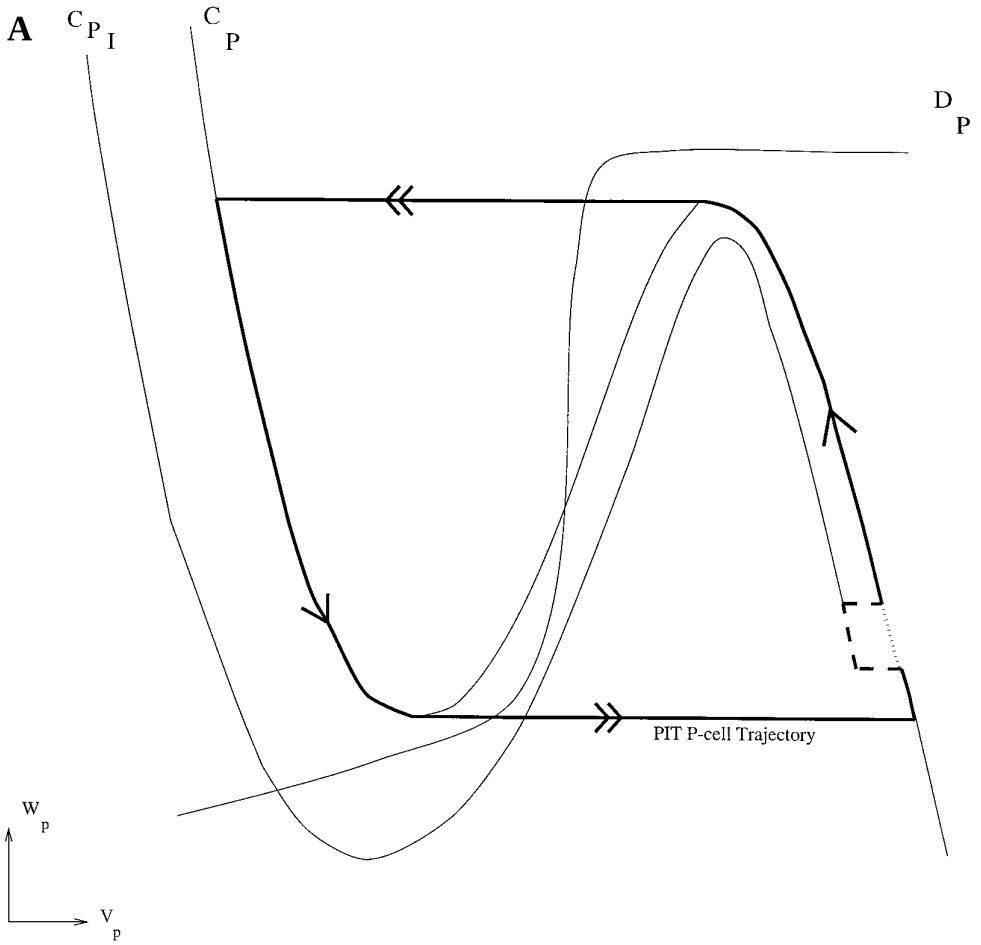

Figure 6. A: The trajectory of the precessing P cell is shown in the case that $\tau_{I_{on}}$ is short. B: A depiction of the inhibition from T "chasing" I around its phase plane. The figure shows how this inhibition changes at each cycle beginning on the right branch and culminating near the knee of the left branch. C: The trajectory of the precessing P cell is shown in the case that $\tau_{I_{on}}$ is long. The intrinsic P cell trajectory is also superimposed. The solid bold curves represent places where these two trajectories coincide. The dashed line corresponds to the precessing P cell and the dotted line to the intrinsic P cell. The time k_r is the time along the right branch of C_P from the right knee of C_{P_I} to the right knee of C_P. The time k_l is the time to cover this same distance, now on the left branch of C_P. The time $\bar{m}$ is the time to cover the dashed portion on the left branch of C_{P_I}, and m is the time to cover this same difference in w values along the dotted portion of the left branch of C_P.

(*Continued on next page*).

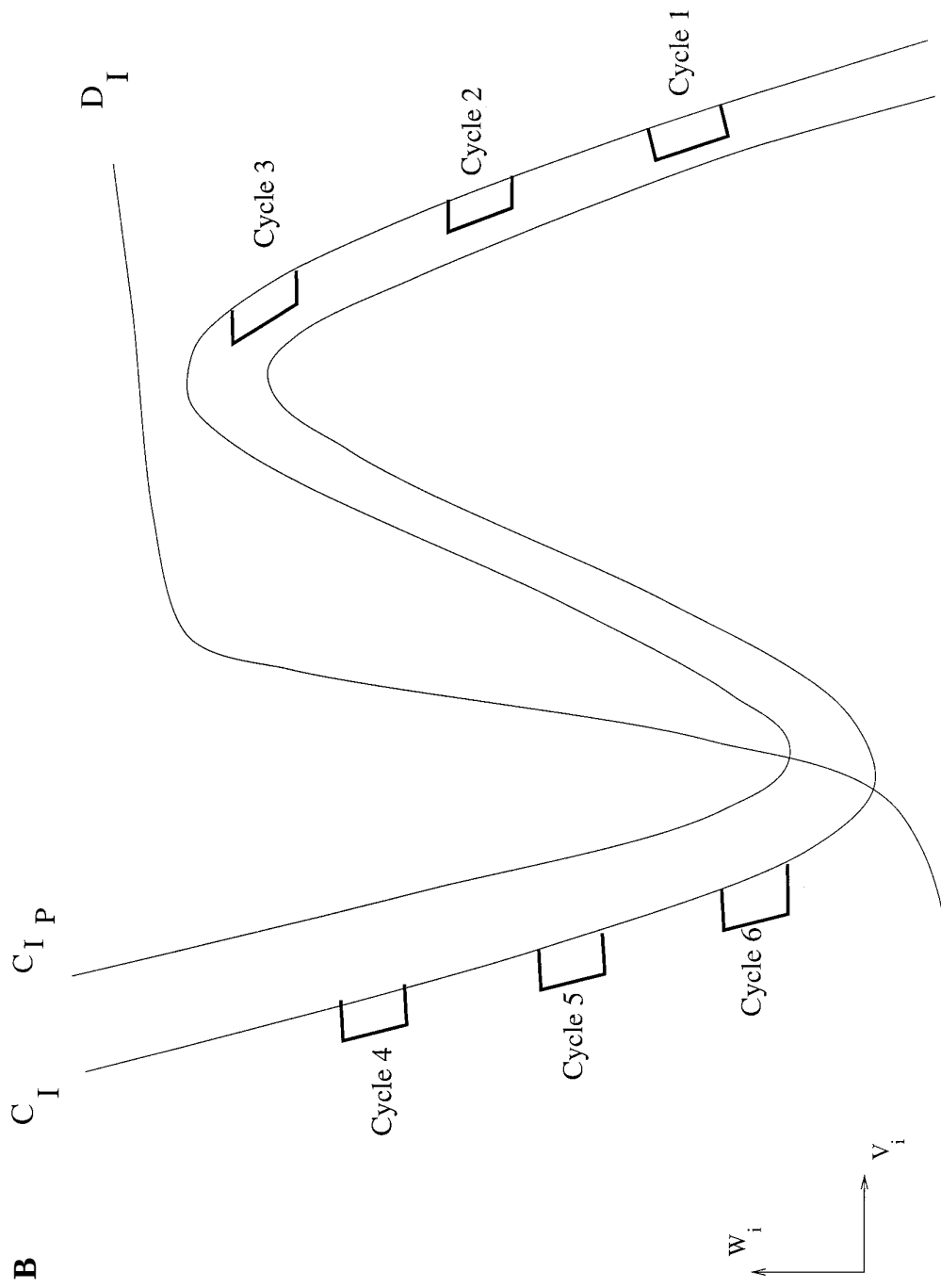

Figure 6. (*Continued on next page*).

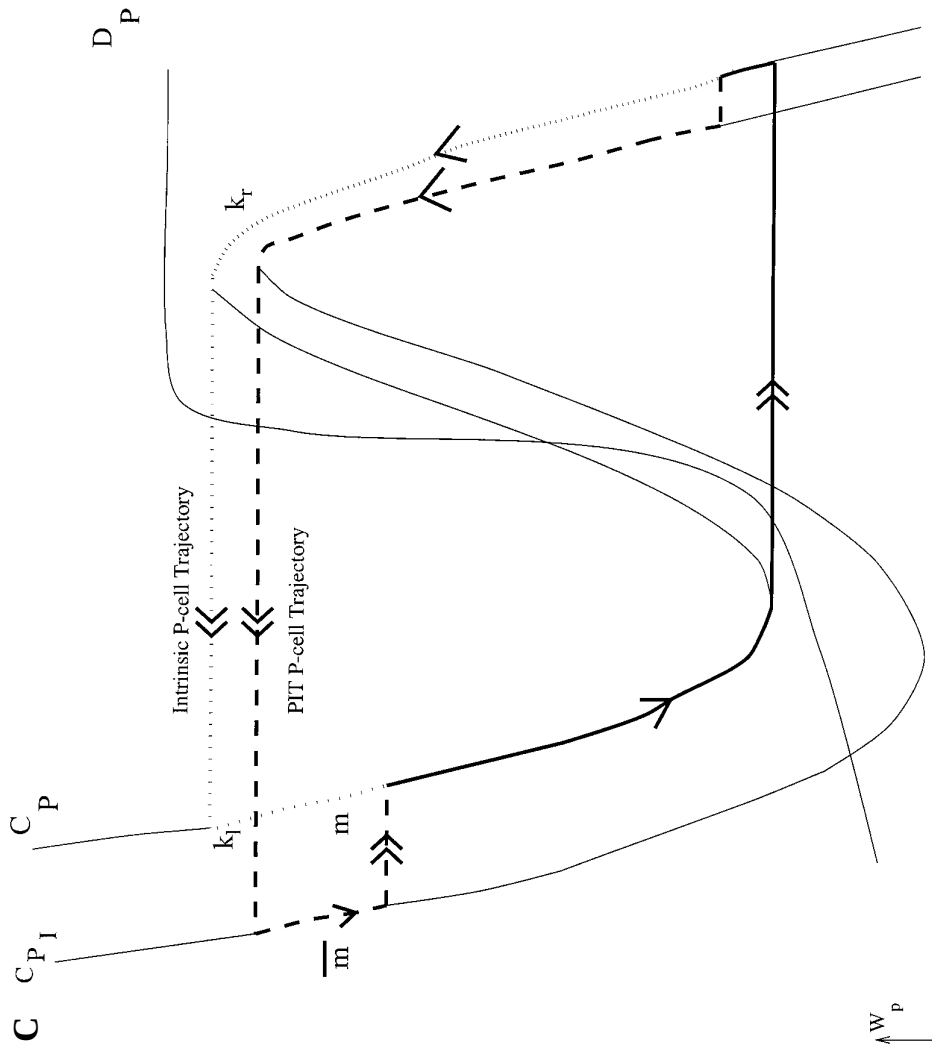

Figure 6. (*Continued*)

unchanging trajectory of P, the trajectory of I changes with each cycle of the precession. As we noticed in Fig. 4, the inhibition from T to I occurs at progressively earlier phases during *PIT*. In terms of the phase portrait (see Fig. 6B), this means that the inhibition from T to I occurs at different places in phase space. In particular, during the first cycle, T inhibits I when I is on the right branch of C_{I_p} and still far away from the right knee. At the next cycle, T inhibits I while I is still on the right branch but now closer to the right knee at a higher w_i value. Progressing in this manner, the inhibition from T eventually occurs when I is back on the left branch but still refractory. Ultimately, I receives inhibition when it is close enough to the left knee of C_I to be captured into *TIP*, thus ending precession and signaling the end of the place field.

Phase precession occurs for a more complicated reason when $\tau_{I_{on}} > \tau_{PA}$. In this case, we assume that P reaches the right knee of C_{P_l} before the inhibition from I shuts off. Note that the right knee of C_{P_l} lies *below* the right knee of C_P. So the length of time P stays in its active state during the *PIT* orbit is less than the length of time it stays in its active state during the *TIP* orbit. This decrease in time is the primary reason why, in this case, phase precession occurs. This can be seen by considering the phase plane of P. There are several subcases depending on the time length of $\tau_{I_{on}}$ (see Appendix A for details). In Fig. 6C, we have drawn the trajectory that P follows one cycle after the seed is given for one of these subcases. Let $\tau = \tau_1$ be the time P hits the right knee of C_{P_l}. Then P jumps back to the left branch of C_{P_l} and evolves down C_{P_l} until $\tau = \tau_1 + \sigma_{pi} + \sigma_{ip}$. We have denoted by lowercase letters various times of evolution for the uncoupled P cell and the coupled precessing P cell. Note that $T_P - T_{\bar{P}} = k_r + k_l + m - \bar{m}$. There are two sources of time reduction. The larger of the two is the time $k_r + k_l$. This time is related to the maximum conductance for the synaptic current from I to P, g_{ip}. If g_{ip} is small, then the cubic C_{P_l} will not be too far below C_P, and thus the time $k_r + k_l$ is small. As g_{ip} increases, so does $k_r + k_l$. The second source of time reduction, and thus phase precession, arises due to the difference $m - \bar{m}$. This difference is controlled by the magnitude of $\frac{\partial g_P}{\partial v_p}$ near the left branch of C_P. For this case, phase precession in the *PIT* orbit is achieved whether Ω is positive, negative, or zero.

3.2.3. The Memory Seed Initiates Phase Precession. Granule cells in the dentate gyrus make excitatory synapses on CA3 pyramidal cells, and granule cells have a spatially specific (Jung and McNaughton, 1993) and theta rhythm phase specific (Skaggs et al., 1996) firing pattern. In our model, the arrival time of the excitatory input, representing the memory seed from these granule cells, need not be so precise. In fact, there exists an open interval of potential seed timings (or phases) that result in phase precession. The seed must be timed to arrive when P is sufficiently close to the left knee of C_P. To determine an expression for the appropriate seed arrival time τ_{seed}, let T fire at $\tau = 0$ and assume that the duration of the seed is small. The seed excitation momentarily adds a current of magnitude $g_{dg}[v_p - v_{dg}]$ to the current balance equation for the P cell, where g_{dg} is the maximal conductance. Phase precession occurs if the seed arrives at $\tau_{seed} \in (-\delta, \tau_{T_{on}} + \sigma_{ip})$ where $\delta > 0$. The lower bound $-\delta$ is related to the parameter g_{dg}. For larger values of g_{dg}, $-\delta$ can be larger (in magnitude). The upper bound on τ_{seed} is a sufficient condition for phase precession since the P cell will certainly precess if it is excited before it receives inhibition from I. As this interval for τ_{seed} gives only a sufficient condition, seeds that arrive slightly after $\tau_{T_{on}} + \sigma_{ip}$ may actually produce phase precession.

3.2.4. The Total Amount of Phase Precession Depends on the Phase of Memory Seed Arrival. In addition to determining whether phase precession is initiated, the timing or phase of the memory seed also affects the total amount of phase change in the P cell during its precession. Since both P and I phase precess and since, in the *TIP* orbit, both cells fire at different fixed phases after T, we need to consider the amount of precession for each of these cells separately.

First consider P. If T fires at $\tau = 0$, then during the *TIP* orbit, P fires at $\tau = \tau_{T_{on}} + \sigma_{ip} + \tau_{I_{on}}$. We can translate these times of firing to phases of firing by multiplying the times by $360^\circ / T_T$. The earlier the seed arrives, with respect to the time of P firing, the smaller the amount that P precesses. Let $\tau_{adv} = \tau_{T_{on}} + \sigma_{ip} + \tau_{I_{on}} - \tau_{seed}$ be the amount of time (or phase) the firing of P is advanced by the memory seed. The total amount of phase precession is a decreasing function of τ_{adv}. In particular, if the seed arrives in the interval $(-\delta, 0)$ (that is, if τ_{adv} is large), P precesses through less than 360 degrees. Whereas if the seed arrives close to $\tau = \tau_{T_{on}} + \sigma_{ip}$ (τ_{adv} small), P precesses through close to 360 degrees, provided that the duration of inhibition from I to P, $\tau_{I_{on}}$, is sufficiently short. Theoretically, the P cell can only phase precess through a full 360 degrees

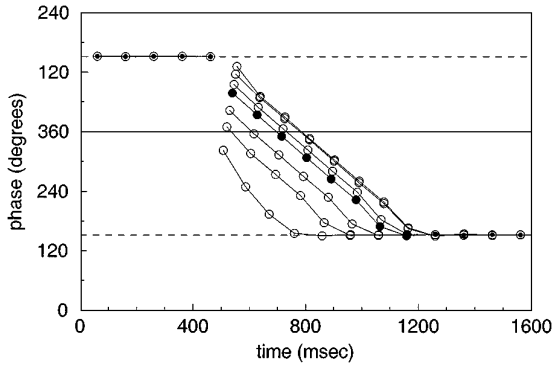

Figure 7. Amount of phase traversed by the P cell during phase precession in the Morris-Lecar-based network model. When zero phase is defined by the peak of the T cell spike, P cell fires (burst times indicated by circles, filled circles indicate Fig. 4 results) at 152 degrees during *TIP* (first five bursts). Seeds arriving earlier (first seed at 500 msec) result in less phase precession than seeds arriving later (last seed at 550 msec). Note also that the number of cycles of phase precession increases with later seed arrival.

in the limit $\tau_{seed} \to \tau_{T_{on}} + \sigma_{ip} + \tau_{I_{on}}$ from below. For $\tau_{I_{on}}$ large, such a seed would fall well outside of the interval described in Section 3.2.3 and thus would be unlikely to produce phase precession. Thus, a lower bound on the maximal amount of phase precession is $360^\circ(1 - \frac{\tau_{I_{on}}}{T_T})$.

An example of the effect of the seed timing on the amount of phase precession is shown in Fig. 7 for the Morris-Lecar-based network model. In the figure, the filled circles indicate the phase of each P cell burst during the *TIP* and *PIT* orbits displayed in Fig. 4. During *TIP*, P fires at approximately 152 degrees (dashed horizontal lines) when 0 degrees is defined by the T spike. The memory seed advances P cell firing to approximately 77 degrees and then P precesses through 285 degrees until returning to the *TIP* orbit and resuming firing at 152 degrees. The open circles indicate the phase of P firing when the seed arrives at different times. For the earliest seed arrival, P precesses through approximately 170 degrees, and for the latest seed, P precesses through roughly 340 degrees.

In contrast to the restriction on the amount of phase precession of the P cell, the I cell can precess through the full 360 degrees. This is possible if $\tau_{seed} \in (\tau_{T_{on}} - \sigma_{pi}, \tau_{T_{on}} + \sigma_{ip})$. The lower bound occurs if the seed arrives at such a time so that the excitation from P to I arrives exactly at the moment T releases I from inhibition.

3.2.5. The Number of Cycles of Phase Precession Depends on the Phasing of the Memory Seed and on the Duration of the Inhibition from I to P. There are two possible formulae for the number of cycles of precession. The duration of inhibition from I to P, $\tau_{I_{on}}$, determines which of the two formulae applies to a given situation. In the case $\Omega > 0$ ($T_P < T_T$), either formula may apply with $\tau_{I_{on}}$ actually determining which one to use. If $\Omega < 0$ ($T_P > T_T$), then only the second formula can be used.

If $\tau_{I_{on}} < \tau_{PA}$, recall from Section 3.2.2, that the *PIT* orbit exists only for $\Omega > 0$. The number of cycles is given simply by

$$n = \frac{T_T - \tau_{adv}}{\Omega}, \tag{12}$$

where n is the nearest integer to the ratio value. Here, it is the difference between the intrinsic periods of T and P, together with τ_{adv}, that determines the number of cycles of precession. The network model that displayed the results in Figs. 4 and 7 generates a *PIT* orbit by satisfying these conditions on Ω and $\tau_{I_{on}}$ and the number of cycles of phase precession is accurately predicted by (12), as shown in Table 2. The values $T_T = 100.3$ ms and $T_P = 87.4$ ms were used.

If Ω is negative with $\tau_{I_{on}} < \tau_{PA}$, then after the seed, (12) predicts and simulations corroborate (not shown) that the P and I cells phase *recess* back to the *TIP* periodic orbit.

If $\tau_{I_{on}} > \tau_{PA}$, as described in Section 3.2.2, there is no requirement on the sign of $\Omega = T_T - T_P$ to obtain the *PIT* orbit. In this case, the number of cycles of phase precession is given by the following expression where the times are defined in Fig. 6C:

$$n = \frac{T_T - \tau_{adv}}{\Omega + k_r + k_l + m - \bar{m}}. \tag{13}$$

Recall that the quantity $k_r + k_l + m - \bar{m}$ is positive, which compensates for a potentially negative Ω. The

Table 2. Number of cycles of phase precession predicted by Eq. (12) and observed in simulations of Morris-Lecar-based network (parameters as in Figs. 4 and 7) for different arrival times of the memory seed.

τ_{adv} (ms)	54	39	29	19	14	9	3
$n_{predicted}$	4	5	5	6	7	7	8
$n_{observed}$	4	5	6	7	7	8	8

time $m-\bar{m}$ is related to the magnitude of $\frac{\partial g_p}{\partial v_p}$ near the left branch of C_P. The magnitude of the time $k_r + k_l$ is of the order of g_{ip} and arises because the burst width and interburst interval are longer for the isolated P cell than in the *PIT* orbit. We ran several simulations (not shown) of the Morris-Lecar-based network model with $T_P > T_T$ (specifically, $T_T = 100.3$ ms and $T_P = 102$ ms). With $g_{ip} = 1.0$, we found $n = 18$, and for $g_{ip} = 1.5$, $n = 9$, thus corroborating the strong dependence of the number of cycles of phase precession on g_{ip}.

Reiterating, if $\Omega > 0$, either (12) or (13) may hold depending on the duration of the inhibition from I to P. By continuous dependence on parameters, there exists an intermediate value for $\tau_{I_{on}}$ at which the network switches from (12) to (13). Note that near this switching point, small changes in the active duration of I have large ramifications with respect to the occurrence of precession and to the number of cycles of precession.

3.2.6. The Spatial Correlation of Phase Precession Is a Speed-Corrected Temporal Phenomena. Other models of phase precession rely explicitly on the assumption that phase precession is a spatial phenomena. We show here that the apparent spatial dependence of phase precession can be accounted for by our temporal model. More precisely, if the interburst frequency of the place cell and the frequency of the underlying theta rhythm are linear functions of the animal's speed, then phase precession can be a temporal phenomenon and also be more correlated with the animal's location than with the time that has passed since it entered the place field.

Assume the linear relationship $f_T = f_B + \gamma_1 v$, $f_{\bar{P}} = f_B + \gamma_2 v$, where f_T is the theta frequency, $f_{\bar{P}}$ is the frequency of the precessing P cell and $\gamma_2 > \gamma_1$ are positive constants. The velocity v is set to $v_0 + \Delta v$, where v_0 is the minimum velocity needed for the theta rhythm to exist, and Δv is the positive deviation from this baseline velocity. Without loss of generality, the frequency f_B is a common baseline for $\Delta v = 0$. Let $\gamma = \gamma_2 - \gamma_1$, then $f_{\bar{P}} = f_T + \gamma v$, where $\gamma > 0$. The time of the nth theta cycle peak is nT_T, and the time of the nth P cell burst, τ_n, is $nT_{\bar{P}} = \frac{nT_T}{1+T_T\gamma v}$. The amount of phase shift after the nth burst ϕ_n is the difference $nT_T - nT_{\bar{P}}$ divided by the period of the theta rhythm; thus $\phi_n = 360^\circ \frac{nT_T\gamma v}{1+T_T\gamma v}$. The position of the rat at the time of the nth burst is $x_n = v\tau_n = \frac{vnT_T}{1+T_T\gamma v}$. By inspection, $\phi_n = 360^\circ \gamma x_n$, or equivalently, the phase is spatially correlated.

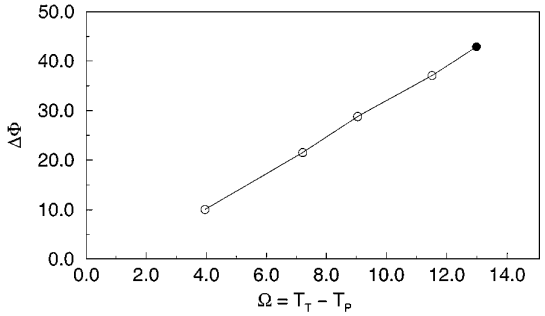

Figure 8. Phase shift of P firing during each cycle of precession changes linearly with changes in animal's running speed, modeled by changing intrinsic frequency of P. In Morris-Lecar-based network model, phase difference of P bursts during precession (circles, filled circle corresponds to Fig. 4 results) increased linearly as intrinsic period of P was decreased, corresponding to an increase in Ω (applied current to P, $I_p = 95$, 98, 100, 103 and 105 $\mu A/\text{cm}^2$). The period $T_T = 100$ ms was fixed throughout.

The phase shift at each cycle is given by $\Delta\phi = 360^\circ \frac{\Omega}{T_T}$. Thus the phase shift is a linear function of the difference in period, and for fixed T_T it is a linear function of T_P. This linear relationship holds in our Morris-Lecar-based network model as shown in Fig. 8. The filled circle showing the largest phase shift during each cycle of phase precession corresponds to the parameter values in Figs. 4 and 7. To model a decrease in running speed, the intrinsic frequency of the P cell was decreased. In response to this increase in T_P, corresponding to a decrease in Ω, the phase shift $\Delta\phi$ decreases linearly.

3.2.7. Suppression of Out-of-Place Field Firing. The primary objective of our model is to illustrate a mechanism for generating the phase precession of place cells. In the model, phase precession only occurs in the place field, but the out-of-place field firing is too high. This implies that a downstream phase-based detector could precisely determine the animal's location at all phases except for the phase-locked one.

Different complicated features could be added to the model to reduce or remove the out-of-place field firing. For example, there are many types of interneurons in the CA3 region that have a diverse pattern of connections and an incompletely determined role in network activity. In particular, some of the interneurons make synaptic connections only on other interneurons (Freund and Buzsáki, 1996). By introducing one additional interneuron into our current model,

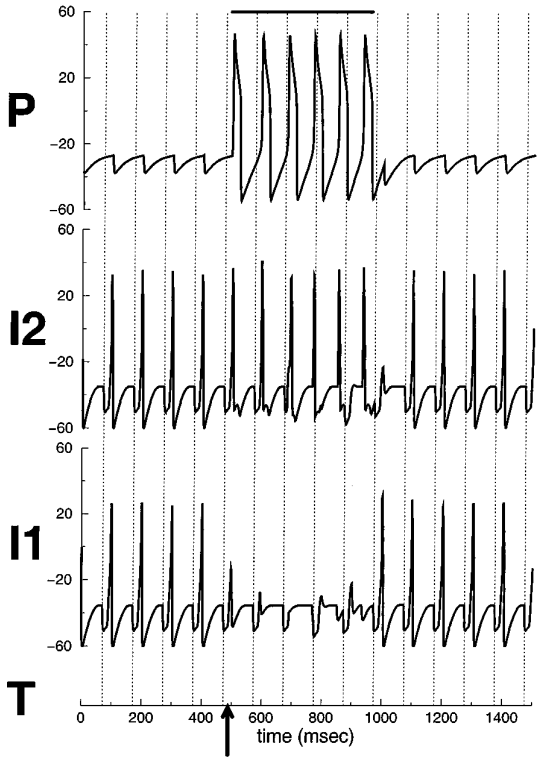

Figure 9. The voltage traces for the three cell and pacemaker network. Phase precession begins at t roughly equal to 500 msec with the arrival of the memory seed. The cells P and I_2 then phase precess for the next 6 cycles. Outside of the place field, the longer lasting inhibition from I_1, which is periodically reinforced, forces P to stay below threshold.

the out-of-place field firing can be suppressed as shown in Fig. 9. In this more complex model T and P are as before, but now there exist two interneurons, I_1 and I_2. Both interneurons receive fast GABA-mediated inhibition from T and are capable of firing rebound spikes. The interneuron I_1 now provides a slowly decaying GABA-mediated inhibitory current to P and receives a similar current from I_2. The interneuron I_2 receives fast glutamatergic excitation from P. As before, P may also have a feedback connection from I_2 that can either be a fast or slow inhibitory current. With this network architecture, we require that the slow inhibition decay in roughly one theta cycle—that is, roughly 100 msec.

Outside of the place field, I_1 and I_2 fire by postinhibitory rebound in response to T. Note that the synaptic delay from I_2 to I_1 allows the latter to rebound before the inhibition from I_2 can take effect. Moreover, this slow inhibition decays away over one theta cycle thus allowing I_1 to again be in a position to fire by rebound. The inhibition from I_1 to P, which lasts the entire theta cycle is strong enough to prevent P from firing during the cycle. Since this inhibition is renewed at each cycle, P never fires. We call this the $TI_1I_2\{P\}$ orbit and note that T controls the dynamics of the network.

As in the simple model, the externally provided memory seed fires P and interrupts the $TI_1I_2\{P\}$ orbit. Excitation from P causes I_2 to fire. The subsequent slowly decaying inhibition from I_2 to I_1 now comes before the fast inhibition from T. Thus I_1 is strongly inhibited and initially will be unable to respond to T input. In the reorganized $PI_2\{I_1\}T$ orbit, phase precession occurs with P controlling I_2 directly, causing it to fire with each P burst and thus phase precess. In this orbit, P also controls I_1, indirectly through I_2. As in the simple model, the timing and effect of the input from T to both I_1 and I_2 changes from cycle to cycle. The effect on I_2 is similar to that discussed in Section 3.2.2 and shown in Fig. 6B. The inhibition from T chases I_2 around its phase plane. When I_2 has precessed through up to 360 degrees, it can be recaptured by T. For precession to end, however, I_1 must be recaptured by T.

Because P and I_2 are phase precessing, the inhibition from I_2 to I_1 comes at progressively earlier phases. This means that at each cycle of theta, there exists progressively more time for this inhibition to decay before the T input to I_1 arrives. Similar to the basic model, phase precession ends when T recaptures control of I_1. This occurs when the input from I_2 to I_1 comes early enough in the T cycle so that the inhibition decays away sufficiently to allow I_1 to rebound in response to T input. Once this happens, the slow inhibition from I_1 to P is reinitiated, thus suppressing P. Moreover, since P has been functionally removed from the circuit, I_2 must now wait for T input to fire. As discussed above, this input occurs at a phase that allows I_1 to fire periodically.

The complex model described here operates in a fundamentally similar fashion to the basic *TIP*/*PIT* model. As before, the role of inhibition differs inside and outside of the place field. Indeed, control of the network of interneurons is again crucial for determining the network output. Moreover, our analytical results in Sections 3.2.2 through 3.2.6 carry over with little or no modification. In this model, it appears that I_1 has an "antiplace field" in that it fires everywhere except

within the place field. In a less reduced and more realistic network model, this may not be the case. As a result, we do not intend our results to be interpreted as predicting the existence of antiplace fields.

4. Discussion

We described a minimal biophysical model of the phase precession of hippocampal place cells that is consistent with the essential empirically determined properties of the phenomenon. We identified mechanisms whereby temporal control of phase precession can occur. In particular, we proposed a mechanism for changing the firing pattern of place cells as the animal enters, crosses, and then leaves the place field. This mechanism of changing control of the interneuron from T to P switches the network from a stable state to a transient state. The precession of the interneurons provides a second mechanism to switch the control of the interneuron back to T and thus return the network to a stable state.

The initial form of the model accounts for most of the empirical observations that were listed in the introduction. Namely, (1) since we provide the seed only when the rat moves in one direction, place cells only fire in one direction of motion; (2) all place cells, only the single P cell in our case, start firing at the same initial phase; (3) the initial phase is the same on each entry of the rat in the place field since the seed always occurs at the same phase; (4) since the change in control in the network occurs before 360 degrees of precession, it is impossible for there to be more than this amount of phase precession; (5) while the cells in the dentate gyrus may undergo a small number of cycles of precession, our model requires only one cycle; additional cycles would not change the results; (6) the model does not account for the increase in firing rate (a less reduced network model that accounts for individual spikes may be able to include firing rate information; we believe that the mechanisms we have uncovered for phase precession in our idealized bursting neurons would carry over to neurons that instead exhibit bursts of spikes); and (7) the linear dependence on frequency of pyramidal cell firing is used here to maintain a correlation with location rather than time that has passed since the animal entered the place field.

The initial model, however, had a high out-of-place field firing rate. This out-of-place field activity would result in a loss of spatial specificity if a downstream system uses firing rate to determine the animal's location in the environment. However, the phase relationship between place cell activity also provides information on the location of the animal, and the background firing outside of the place field may not be a substantial problem for a downstream system that uses phase to determine the animal's location. We presented a method (not necessarily unique), using an additional interneuron, to remove the out-of-place field firing without requiring upstream information on the size and extent of the place field.

From a mathematical point of view, this work shows the importance of determining functionality of the subpieces of the model. We have shown how control within the network can be switched from one network member to another and then back again. We have demonstrated that geometric analysis is well suited to identify the mechanisms that change control. Our work also highlights the changing and perhaps nonintuitive effects of inhibition in the network. In particular, we have shown how a faster oscillator can entrain a slower one using only inhibition. This depends critically on the timing of the inhibitory input from the faster oscillator, which is consistent with the theme that timing is of fundamental importance in temporal code generation. We have also shown how the network can use inhibition to functionally enhance or remove the effects of a chosen member.

4.1. Related Work

Other models of phase precession differ from ours in important ways. In prior work (Tsodyks et al., 1996; Jensen and Lisman, 1996; Wallenstein and Hasselmo, 1997; Kamondi et al., 1998), phase precession is modeled as a spatial phenomena. Each of these models in some way utilizes external input that already encodes for the phase precession. Thus none of the models truly explains the genesis of phase precession. Namely, the models do not address how a single P cell behaves both outside and inside its place field or what causes the transition in behavior of the cell between these two areas.

The above models require either a network of excitatory cells or a highly parameterized description of the neuron to achieve precession. In the work of Jensen and Lisman (1996), a one-dimensional chain of pyramidal cells is considered, and phase precession occurs due to the local unidirectional excitatory synapses between these cells. Selective excitation to a specific member of the chain, occurring at each theta cycle, provides phase-precessed input to the network. In the model of

Tsodyks et al. (1996), strong excitatory connections between place cells is also required. In this model, precession is driven by asymmetric synaptic weights between these cells. The total amount of excitatory input a cell receives is at a maximum in the center of the place field and decreases monotonically as the distance from the center increases. Tsodyks et al. (1996) call this "directional tuning." A similar idea is employed by Kamondi et al. (1998). There a ramplike depolarizing current is provided to the place cell to mimic passage through the place field. Thus in these two models, the running animal is given external information about its position in space that is encoded in the spatially dependent depolarization. Kamondi et al. (1998) and Wallenstein and Hasselmo (1997) both use multicompartment descriptions of the place cells. Precession in these models depends critically on a more complex, multiparameter description of each neuron. Moreover, the model of Wallenstein and Hasselmo (1997) also requires phase-precessed external input at each theta cycle as in Jensen and Lisman (1996) to achieve precession.

The present model takes an entirely different approach. First, we believe phase precession is a temporal mechanism that, as demonstrated, can account for changes in the rat's running speed. Second, we do not require any external precessed input to the network. Instead, we simply need a one time dose of excitation that mimics a memory seed and changes the network from the *TIP* to the *PIT* orbit. We do not require a network of excitatory cells or multicompartment models for the cells. Finally, our analysis gives a different interpretation of the significance of phase precession than all of the previous studies. Namely, in our model the end of phase precession signals the end of the place field. In the other studies, the end of the place field signals the end of the precession. Thus our model provides an internal mechanism for determining the end of the place field (via the end of precession), whereas the other models require another external input to notify the pyramidal cell that its place field has ended.

4.2. Experimental Support

Several studies have demonstrated that the mean phase of activity of hippocampal interneurons is just prior to the mean phase of pyramidal cell activity (Fox et al., 1986; Buzsáki and Eidelberg, 1982). This implies that during the phase precession, the activity of a place cell must pass through the phase of theta rhythm at which interneurons are most strongly inhibiting pyramidal cells. In the present model the pyramidal cell controls the firing of the interneuron during the phase precession process, and its activity is not adversely inhibited by the interneuron.

In recent recordings of a larger number of pyramidal cells and interneurons (Csicsvari et al., 1998), pyramidal cells were found that had large, significant cross-correlation peaks at times on the scale of ten milliseconds that preceded the activity of simultaneously recorded interneurons. These correlations find that there is a tight coupling in the time at which pyramidal cells and interneurons are active and suggests that the activity of a subset of the interneurons might precess along with place cells. The experimental evidence of the high level of correlation between place cells and interneurons demonstrates that there exists a sufficiently strong conductance between subsets of these two types of neurons. These findings are consistent with the predictions in the present model in which the phase precession of interneurons may only occur in a subset of interneurons and only when they are being driven by a phase precessing place cell.

4.3. Consistency of Biophysical and Functional Models

In a model of phase precession, there are several important larger goals and anatomical considerations that should be taken into account. There is considerable data that demonstrates that the hippocampus has a role in episodic memory. We have proposed a functional model that describes how the spatial and memory roles of the hippocampus can be combined (Recce and Harris, 1996; Recce, 1999). In this view, when a rat returns to a previously experienced environment, the set of coactive place cells corresponds to the recall of an egocentric map of the environment. The memory recall is performed by a pattern completion process that is controlled through the excitatory feedback pathway in the CA3 region of the hippocampus. The seed for this recall enters the CA3 region through the entorhinal cortex to the dentate gyrus and then in the mossy fiber projection from the dentate granule cells to the CA3 pyramidal cells and interneurons. The temporal control of the recall process, in this view, is provided by the pacemaker input from the medial septum.

The feedback connections between CA3 pyramidal cells are relatively sparse, which can limit the number of egocentric maps of space that can be stored if

the region is modeled as an autoassociative memory. However, Gardner-Medwin (1976) has demonstrated that this limitation can be overcome if the recall process is performed over a sequence of steps. Hirase and Recce (1996) found that the optimal performance in a multistep autoassociative memory model of the CA3 region can be achieved if an interneuron network controls the recall process by providing an inhibitory input to the pyramidal cells that is a linear function of the number of simultaneously active pyramidal cells. Further, it has been proposed that the phase precession corresponds to the multiple steps in this recall process and that the phase precession suggests a method for the concurrent recall of several egocentric memories (Recce, 1999).

In the present work, we have begun the process of systematically addressing these issues. The present model for phase precession, while conceptually quite simple, is not necessarily the one that most easily produces output that phase precesses. Instead, our modeling is based on the larger considerations of identifying mechanisms that can allow multiple memory recall processes to be simultaneously performed. The basic framework described above, which accounts for precession, is compatible with a functional model of the spatial and episodic memory roles of CA3 place cells.

Appendix A. Analysis: Existence and Stability of *TIP* Periodic Orbit

Outside the place field, the network is in the *TIP* configuration. We show that there is a unique, stable periodic orbit to which the cells are attracted. Assume that T fires at $\tau = 0$. We will locate an initial condition for P and show that when T fires again at $\tau = T_T$, P has returned exactly to this initial condition. The analysis will be in terms of a time metric that will measure the times of evolution of P on various parts of its orbit in phase space. These times depend on various biophysical parameters that are related to both intrinsic and synaptic properties of the cells and the network.

Theorem 1. *There exists a locally unique asymptotically stable TIP periodic orbit with a period $O(\epsilon)$ close to T_T.*

Proof The analysis below occurs at $\epsilon = 0$, but using the work of Mischenko and Rozov (1980), the results actually hold for $\epsilon > 0$ and sufficiently small. Consider the left branch of C_P between w_{RK} and w_{LK}. Associated to each point on this curve, denoted w_p, is the time $\Delta(w_p)$ it takes P to reach w_{LK} starting from w_p. In particular, $\Delta(w_{RK}) = \tau_{PR}$ and $\Delta(w_{LK}) = 0$. It is clear that Δ is a monotone decreasing function of w_p. The description of the *TIP* network given earlier shows that there is a one-dimensional map Π that takes the initial position of P at $\tau = 0$ along the left branch of C_P and returns the position of P at $\tau = T_T$.

Proposition 1. *The map Π defines a uniform contraction on a subinterval (w_{lo}, w_{hi}) of (w_{LK}, w_{RK}). If $w^\star$ is the resulting locally unique asymptotically stable fixed point , then the network possesses a locally unique asymptotically stable singular TIP periodic orbit with period T_T, where $w_p(0) = w^\star$.*

Proof We prove the existence of a fixed point by comparing the behavior of the uncoupled P cell to its coupled counterpart. Since $T_T = T_P + \Omega$, we can compare the period of the coupled P cell to T_T. First we locate a suitable w_{hi}. Associated with it is a time T_{hi} from w_{hi} to w_{LK} on C_P. At $\tau = \tau_{T_{on}} + \sigma_{ip}$, P receives inhibition and jumps back to C_{P_l}. At $\tau = \tau_{T_{on}} + \sigma_{ip} + \tau_{I_{on}}$, the inhibition to P shuts off. We choose w_{hi} such that $w_p(\tau_{T_{on}} + \sigma_{ip} + \tau_{I_{on}}) = w_{LK}$. Next let us consider the evolution of the P cell, solely on C_P in the absence of any synaptic input. Since $\frac{\partial g_p}{\partial v_p} > 0$ near the left branch of C_P and C_{P_l}, the P cell moves down C_P at a slower rate than on C_{P_l}. In other words, P takes a longer time to cover the same Euclidean distance on C_P than on C_{P_l}. Thus at $\tau = \tau_{T_{on}} + \sigma_{ip} + \tau_{I_{on}}$, the uncoupled P cell will be above w_{LK}. It is seen that inhibition actually shortens the time distance to the knee for this initial condition. This is very similar to, but timewise the opposite of, the idea of virtual delay of Kopell and Somers (1995). There they showed that excitation had the opposite effect of increasing the time to the knee. The coupled and uncoupled versions of P follow the same trajectory in the active state.

Assume momentarily that $\Omega = 0$. For the uncoupled P cell, $\Delta(\Pi(w_{hi})) = T_{hi}$. But for the coupled P cell, $\Delta(\Pi(w_{hi})) < T_{hi}$. Thus the time it takes for the coupled P cell to return to its initial position w_{hi} is $T_{pc} < T_P$. If Ω is sufficiently small, then $T_{pc} < T_P + \Omega = T_T$. Note that $T_{hi} > \tau_{T_{on}} + \sigma_{ip} + \tau_{I_{on}}$. How big the difference between these times needs to be depends on the size of $\frac{\partial g_p}{\partial v_p}$, which determines the difference in the rates along C_P and C_{P_l}. Thus we have located an initial condition whose time distance to the knee compresses over one oscillation.

We next locate an initial condition whose time distance to the knee expands. Now let $w_{lo} = w_p(0)$ such

that for the uncoupled P cell $w_P(\tau_{T_{on}} + \sigma_{ip}) = w_{LK}$. Assume that the initial conditions for T and I are identical to the above case. Thus at the moment P were to fire, it receives inhibition from I. It will thus fall back to C_{P_I} and move down this cubic toward the fixed point on C_{P_I} for a time $\tau_{I_{on}}$. At $\tau = \tau_{T_{on}} + \sigma_{ip} + \tau_{I_{on}}$, P is released from inhibition and jumps to the right branch. The w value of the point to where it jumps lies below w_{LK}. On the the right branch, let the time between this point and w_{LK} be denoted by τ_D. Once P passes through $w_p = w_{LK}$ on the right branch of C_P, it will follow the same orbit as the uncoupled P cell. The coupled P cell has been delayed by a time $\tau_{I_{on}} + \tau_D$. So it will return to its initial position at a time $T_{pc} > T_P$, if $\Omega = 0$. Thus if Ω is sufficiently small, $T_{pc} > T_T$. For this initial condition, the time distance to the knee has been expanded—that is, $\Delta(\Pi(w_{lo})) > \Delta(w_{lo})$.

Therefore, we have located a set of initial conditions such that the lower and upper boundaries of the set are mapped into the interior of the set by the map Π. By continuous dependence on initial conditions, this implies that there exists at least one element of the set that remains fixed under the map Π. To prove that this point is unique and attracting, we need to show that Π is a contraction mapping. We follow two different versions of the P cell, denoted P_1 and P_2, and show that the dynamics of the *TIP* network bring these cells closer together after one iterate of Π. Let $w_1 < w_2$ denote any two points in (w_{lo}, w_{hi}) such that $w_{p_1}(0) = w_1$ and $w_{p_2}(0) = w_2$. The cells P_1 and P_2 do not interact with one another but receive common inhibition from the same I cell.

Lemma 1. *There exists* $\lambda \in (0,1)$ *such that* $|\Pi(w_2) - \Pi(w_1)| < \lambda |w_2 - w_1|$.

Proof: From the above analysis, it is clear that in the *TIP* network, P_1 and P_2 will jump to the active state from a point on C_{P_I} that lies below the left knee of C_P. This occurs at $\tau = \tau_{T_{on}} + \tau_{I_{on}} + \sigma_{ip}$. Let δ denote the time between the cells at $\tau = 0$. As the cells evolve along the left branch of C_P and then C_{P_I}, the time between them remains invariant. However, the Euclidean distance between the cells decreases. This is a standard fact for two cells that are evolving along the same one-dimensional curve toward a fixed point. The longer the cells spend near the critical point formed by the intersection of C_{P_I} and D_P, the more the Euclidean distance is compressed. At $\tau = \tau_{T_{on}} + \tau_{I_{on}} + \sigma_{ip}$, the cells are released from inhibition and jump horizontally to the right branch of C_P. The same mechanism that fosters synchrony due to fast threshold modulation (see Somers and Kopell, 1993) implies that there is compression across the jump. The rational is the following. Across the jump, the Euclidean distance does not change. However, the rate of evolution of the cells on the left branch is much slower due to the fact that these cells are evolving near a critical point. On the right branch the cells are very far way from the w-nullcline D_p, so the rate of evolution is much faster. Thus the cells travel through the same Euclidean distance in a much shorter time. Thus the new time between cells is less than δ. Since the cells always satisfy the same differential equation, the time between them remains invariant on the right branch of C_P. Moreover, since they both jump down from the right knee of the C_P, the time is invariant across the down jump. When P_1 and P_2 return to the left branch of C_P, P_2 will lie below P_1. So when P_2 returns to the initial position of P_1 at w_1, the time between the cells will be less than when they started, so the Euclidean distance between them must have compressed. This proves that Π is a contraction. The constant λ can roughly be approximated by the ratio of the speed at the jump on point on the right branch to the speed at the jump off point on the left branch (Somers and Kopell, 1993).

We have made some implicit assumptions about the behavior of I. Namely, we have not proved that I actually returns to its initial position at $\tau = T_T$. We are assuming that the time on the left branch of C_I from $w = w_{RK}$ of C_I to a neighborhood of the fixed point on C_I is bounded from below and above. The upper bound arises from the fact that we want I to be able to respond to T at $\tau = T_T$. The lower bound comes from the fact that we do not want I to fire for the time period $\tau_{PA} + \sigma_{ip}$. Provided these conditions are met, the existence of an asymptotically stable fixed point implies the existence of an asymptotically stable singular periodic orbit. It is now fairly standard to show that the map Π perturbs smoothly for $\epsilon > 0$, but sufficiently small, thus yielding the actual *TIP* periodic orbit (Mischenko and Rozov, 1980). □

Let us now address more carefully what we mean by the active state of the interneuron. In *PIT*, it is not possible to locate the precise place from which I jumps up. Thus the precise location at which it reaches the right branch is not determinable, and therefore we cannot precisely define its active duration. To give an estimate first on the jump up point we need to define two more cubics. One is C_{I_p}, which occurs when $s_{PI} = 1$

and $s_{TI}=0$. The second is $C_{I_{PT}}$, which occurs when both $s_{PI}=1$ and $s_{TI}=1$. Note that $C_{I_{PT}}$ lies between C_{I_P} and C_{I_T}. Depending on the parameters g_{pi}, g_{ti}, v_{pi}, and v_{ti}, it may lie above or below C_I. For this argument assume it lies above C_I. Then the maximum w value to which I can jump is the w value of the left knee of C_{I_P}, call it w_{i_M}. The minimum value is the w value of the intersection of C_I and D_I, call it w_{i_m}. Since $\frac{\partial g_i}{\partial v_i}=0$ near the right branches, the speeds of evolution along all the right branches are identical. For this argument the ordering of the right knees of the relevant cubics is $R_{I_T}<R_I<R_{I_{PT}}<R_{I_P}$, where the notation should be clear. So, by a long active phase of the interneuron, we mean the time from w_{i_M} to R_{I_T} is longer then τ_{PA_I}. By a short active phase we mean the time from w_{i_m} to R_{I_P} is less than τ_{PA_I}. Note that these times are simply bounds for the length of the active phase. They do not imply that I necessarily jumps down from a specific knee. Indeed, I's jump down point may change each cycle depending on the timing of inhibition from T. Finally, if the length of the active state of I is too long—for example, if the time w_{i_M} to R_I is much longer than $\tau_{PA_I}+\sigma_{pi}$, then the analysis presented above breaks down. This is because I will not be in a position to respond to the next bout of excitation from P.

Appendix B. Model Equations and Parameter Values

We have numerically implemented our two cell and pacemaker network using the Morris-Lecar equations (1981) to model the neurons. The current balance equations for the P and I cells are

$$\begin{aligned}C_m\frac{dv_p}{dt}&=-g_{Ca}m_\infty(v_p)(v_p-v_{Ca})-g_K w_p(v_p-v_K)\\&\quad-g_L(v_p-v_L)-s_{ip}g_{IP}(v_p-v_{IP})+I_p,\\C_m\frac{dv_i}{dt}&=-g_{Ca}m_\infty(v_i)(v_i-v_{Ca})-g_K w_i(v_i-v_K)\\&\quad-g_L(v_i-v_L)-s_{pi}g_{PI}(v_i-v_{PI})\\&\quad-s_{ti}g_{TI}(v_i-v_{TI})+I_i,\end{aligned}$$

where v_X (in mV) is the membrane voltage in the pyramidal cell ($X=p$) and the interneuron ($X=i$). The maximal conductances for the calcium and potassium currents in the cells are the same ($g_{Ca}=4.4$, $g_K=8.0$). The reversal potentials for the ionic currents are $V_{Ca}=120$ mV and $V_K=-84$ mV. The leak conductance density in each cell is $g_L=2\,mS/\text{cm}^2$, and the leak reversal potential is $V_L=-60$ mV. The membrane capacitance is $C_m=20\ \mu F/\text{cm}^2$. The applied current values (in $\mu A/\text{cm}^2$) are $I_p=105$ and $I_i=120$. In our implementation of the model, the T cell is modeled by the same equations as an isolated P cell, except applied current is set to 92 $\mu A/\text{cm}^2$. In order to obtain frequencies in the theta range, time was scaled by 4.5. The model equations were numerically integrated using XPP (information on the program available at http://www.pitt.edu/∼phase).

The gating kinetics of the potassium conductances in each cell ($X=p$ and i) are governed by equations of the following form:

$$\frac{dw_X}{dt}=\phi\frac{w_{\infty,X}(v)-w_X}{\tau_{w,X}(v)},$$

where $\phi=0.005$ corresponds to ϵ in the general form of the equations. The steady-state activation and inactivation functions and the voltage-dependent time constant functions for the calcium and potassium currents in each cell ($X=p$ and i) are given by

$$\begin{aligned}m_\infty(v)&=\frac{1}{2}\left[1+\tanh\left(\frac{v-v_1}{v_2}\right)\right],\\w_{\infty,X}(v)&=\frac{1}{2}\left[1+\tanh\left(\frac{v-v_{3,X}}{v_{4,X}}\right)\right],\\\tau_{w,X}(v)&=\frac{1}{\text{sech}[(v-v_{3,X})/2v_{4,X}]}.\end{aligned}$$

The half-activation voltages for the gating functions are (in mV) $v_{1,p}=v_{1,t}=-1.2$, $v_{3,p}=2$, and $v_{3,i}=-25$. The activation and inactivation sensitivities for the gating functions are (in mV) $v_{2,p}=v_{2,i}=18$, $v_{4,p}=30$, and $v_{4,i}=10$.

The synaptic currents in each cell are governed by the variable s_{XY} where X indicates the presynaptic cell and Y indicates the postsynaptic cell. These variables satisfy equations of the form

$$s'_{XY}=\alpha(1-s_{XY})\frac{1}{2}\left(1+\tanh\left(\frac{v_X-v_5}{v_6}\right)\right)-\beta\,s_{XY},$$

where the Heaviside function in the general form of the equations for s_{XY} is replaced by a sigmoidlike function that depends on the presynaptic voltage (half-activation $v_5=0$ and activation sensitivity $v_6=10$). For the three synaptic currents in the model, governed by s_{pi}, s_{ip}, and s_{ti}, the rise and decay rates of the synapse are

the same ($\alpha = 2$, $\beta = 1$). In the current balance equations, the effect of the synapse is determined by the reversal potentials of the synaptic currents ($v_{pi} = 80$, $v_{ip} = v_{ti} = -80$), and the maximal conductances of the synaptic currents are all equal ($g_{pi} = g_{ip} = g_{ti} = 1$). We took $\sigma_{ip} = \sigma_{pi} = 0$ in the simulations, thus showing that the existence of delays are not crucial for the above results.

For the simulation in Fig. 9, the following parameters were used: $I_p = 118$, $I_{i_1} = 80$, $I_{i_2} = 80$, $g_{i_2 i_1} = 0.5$, $\alpha_{i_2 i_1} = 5$, $\beta_{i_2 i_1} = 0.005$, $v_{i_2 i_1} = -95$, $g_{pi_2} = 1$, $\alpha_{pi_2} = 2$, $\beta_{pi_2} = 1$, $v_{pi_2} = 80$, $g_{i_1 p} = 0.8$, $\alpha_{i_1 p} = 3$, $\beta_{i_1 p} = 0.001$, $v_{i_1 p} = -95$, $g_{ti_1} = 2.5$, $\alpha_{ti_1} = 2$, $\beta_{ti_1} = 2$, $v_{ti_1} = -80$, $g_{ti_2} = 2.5$, $\alpha_{ti_2} = 2$, $\beta_{ti_2} = 2$, and $v_{ti_2} = -80$.

Acknowledgments

This work was supported, in part, by the New Jersey Institute of Technology under grants 421540 (AB), 421590 (VB), and 421920 (MR). V. Booth also acknowledges support from the National Science Foundation (grant IBN-9722946).

References

Bullock TH, Buzsaki G, McClune MC (1990) Coherence of compound field potentials reveals discontinuities in the calsubiculum of the hippocampus in freely-moving rats. *Neurosci.* 38:609–619.

Buzsáki G, Eidelberg E (1982) Direct afferent excitation and long term potentiation of hippocampal interneurons. *J. Neurophysiol.* 48:597–607.

Csicsvari J, Hirase H, Czurko A, Buzsaki G (1998) Reliability and state-dependence of pyramidal cell-interneuron synapses in the hippocampus: An ensemble approach in the behaving rat. *Neuron* 21:179–189.

Ermentrout GB, Kopell N (1998) Fine structure of neural spiking and synchronization in the presence of conduction delays. *Proc. Natl. Acad. Sci.* 95:1259–1264.

Fox SE, Ranck JB (1975) Localization and anatomical identification of theta and complex spike cells in dorsal hippocampal formation of rats. *Exp. Neurol.* 49:299–313.

Fox SE, Wolfson S, Ranck JB (1986) Hippocampal theta rhythm and the firing of neurons in walking and urethane anesthetized rats. *Exp. Brain Res.* 62:495–500.

Freund TF, Antal M (1988) GABA-containing neurons in the septum control inhibitory interneurons in the hippocampus. *Nature* 336:170–173.

Freund TF, Buzsáki G (1996) Interneurons of the hippocampus. *Hippocampus* 6:347–470.

Gardner-Medwin AR (1976) The recall of events through the learning of associations between their parts. *Proc. R. Soc. Lond. B* 194:375–402.

Gibson WG, Robinson J (1992) Statistical analysis of the dynamics of a sparse associative memory. *Neural Networks* 5:645–661.

Green J, Arduini A (1954) Hippocampal electrical activity in arousal. *J. Neurophysiol.* 17:533–557.

Hirase H, Recce M (1996) A search for the optimal thresholding sequence in an associative memory. *Network* 7:741–756.

Jensen O, Lisman JE (1996) Hippocampal CA3 region predicts memory sequences: Accounting for the phase advance of place cells. *Learn. Mem.* 3:257–263.

Jung MW, McNaughton BL (1993) Spatial selectivity of unit activity in the hippocampal granular layer. *Hippocampus* 3:165–182.

Kamondi A, Acsady L, Wang X, Buzsaki G (1998) Theta oscillations in somata and dendrites of hippocampal pyramidal cells in vivo: Activity-dependent phase-precession of action potentials. *Hippocampus* 8:244–261.

King C, Recce M, O'Keefe J (1998) The rhythmicity of cells of the medial septum/diagonal band of broca in the awake freely moving rat: Relationship with behaviour and hippocampal theta. *Eur. J. Neurosci.* 10:464–467.

Kopell N, Somers D (1995) Anti-phase solutions in relaxation oscillators coupled through excitatory interactions. *J. Math. Biol.* 33:261–280.

Marr D (1971) Simple memory: A theory for archicortex. *Phil. Trans. R. Soc. Lond. B* 176:23–81.

Mishchenko EF, Rozov NK (1980) Differential Equations with Small Parameters and Relaxation Oscillators. Plenum Press, New York.

Morris C, Lecar H (1981) Voltage oscillations in the barnacle giant muscle fiber. *Biophys. J.* 35:193–213.

Muller RU, Kubie JL, Bostock EM, Taube JS, Quirk G (1987) Spatial firing correlates of neurons in the hippocampal formation of freely moving rats. *J. Neurosci.* 7:1951–1968.

Nadim F, Manor Y, Nussbaum P, Marder E (1998) Frequency regulation of a slow rhythm by a fast periodic input. *J. Neurosci.* 18:5053–5067.

O'Keefe J (1976) Place units in the hippocampus of the freely moving rat. *Exp. Neurol.* 51:78–109.

O'Keefe J, Dostrovsky J (1971) The hippocampus as a spatial map: Preliminary evidence from unit activity in the freely moving rat. *Brain Research* 34:171–175.

O'Keefe J, Recce ML (1993) Phase relationship between hippocampal place units and the EEG theta rhythm. *Hippocampus* 3:317–330.

Recce M (1994) The representation of space in the rat hippocampus. Ph.D. thesis, University College London.

Recce M (1999) Encoding information in neuronal activity. In: Maass W, Bishop C, eds. Pulsed Neural Networks. MIT Press, Cambridge, MA. pp. 111–131.

Recce M, Harris KD (1996) Memory for places: A navigational model in support of Marr's theory of hippocampal function. *Hippocampus* 6:735–748.

Rieke F, Warland D, de Ruyter van Steveninck D, Bialek W (1997) Spikes-Exploring the Neural Code. MIT Press, Cambridge, MA.

Rinzel J, Ermentrout G (1998) In: Koch C, Segev I, eds. Methods in Neuronal Modeling: From analysis of Neural Excibability and Oscillations to Networks. 2nd edition. MIT Press, Cambridge, MA. pp. 251–291.

Rubin J, Terman D (2000) Geometric analysis of population rhythms in synaptically coupled neuronal networks. *Neur. Comp.*, 12:597–645.

Skaggs WE, McNaughton BL, Wilson MA, Barnes CA (1996) Theta-phase precession in hippocampal neuronal populations and the compression of temporal sequences. *Hippocampus* 6:149–172.

Somers D, Kopell N (1993) Rapid synchronization through fast threshold modulation. *Biol. Cyber.* 68:393–407.

Terman D, Kopell N, Bose A (1998) Dynamics of two mutually coupled slow inhibitory neurons. *Physica D* 117:241–275.

Terman D, Lee E (1997) Partial synchronization in a network of neural oscillators. *SIAM J. Appl. Math.* 57:252–293.

Treves A, Rolls ET (1994) A computational analysis of the role of the hippocampus in memory. *Hippocampus* 4:373–391.

Tsodyks MV, Skaggs WE, Sejnowski TJ, McNaughton BL (1996) Population dynamics and theta rhythm phase precession of hippocampal place cell firing: A spiking neuron model. *Hippocampus* 6:271–280.

van Vreeswijk C, Abbott L, Ermentrout GB (1994) When inhibition, not excitation synchronizes neural firing. *J. Comp. Neurosci.* 1:313–321.

Wallenstein GV, Hasselmo ME (1997) GABAergic modulation of hippocampal population activity: Sequence learning, place field development, and the phase precession effect. *J. Neurophysiol.* 78:393–408.

Wang XJ, Rinzel J (1992) Alternating and synchronous rhythms in reciprocally inhibitory neuron models. *Neural Comp.* 4:84–97.